Specific ion channels control sensory gain, sensitivity, and kinetics in a tonic thermonociceptor

Specific ion channels control sensory gain, sensitivity and kinetics in a tonic thermonociceptor

Authors:

Gabriella Saro[1], Andrei-Stefan Lia[1], Saurabh Thapliyal[1], Filipe Marques[1], Karl Emanuel Busch[2], Dominique A. Glauser[1*]

[1] Department of Biology, University of Fribourg, 1700 Fribourg, Switzerland

[2] Centre for Discovery Brain Sciences, University of Edinburgh, Edinburgh, EH8 9XD, Scotland

*Corresponding and lead author, dominique.glauser@unifr.ch

Summary

Pain sensation and aversive behaviours entail the activation of nociceptor neurons, whose function is largely conserved across animals. The functional heterogeneity of nociceptors and ethical concerns are challenges for their study in mammalian models. Here, we investigate the function of a single type of genetically identified *C. elegans* thermonociceptors named FLP. Using calcium imaging *in vivo*, we demonstrate that FLP encodes thermal information in a tonic and graded manner over a wide thermal range spanning from noxious cold to noxious heat (8-36°C). This tonic-signalling mode allows FLP to trigger sustained behavioural changes necessary for escape behaviour. Furthermore, we identify specific Transient Receptor Potential, Voltage-gated Calcium, and sodium 'leak' channels controlling sensory gain, thermal sensitivity, and signal kinetics, respectively, and show that the Ryanodine receptor is required for long-lasting activation. Our work elucidates the task distribution among specific ion channels to achieve remarkable sensory properties in a tonic thermonociceptor *in vivo*.

Keywords

thermosensation, heat sensation, cold sensation, TRP, NALCN, VGCC, RyR, optogenetics

Introduction

Nociceptors are peripheral sensory neurons able to detect noxious stimuli, such as extreme temperatures. They encode sensory information and deliver it to downstream neurons in the nervous system to trigger aversive behaviors, which are essential for the protection of the organism. Nociceptors also play an important role in pain perception and, as such, have received considerable attention in the search for improved pain management solutions (Dubin and Patapoutian, 2010). In vertebrates, nociceptors constitute a heterogeneous population of neurons, varying according to their size, their conduction velocity, the type and number of stimuli they are sensitive to, and the molecular components they express (Gold and Gebhart, 2010, Dubin and Patapoutian, 2010). Furthermore, nociceptors include both phasic receptors (activated by changes in stimulus intensity) and tonic receptors (continuously responding during prolonged stimulations) (de Moraes et al., 2017, Yu et al., 2014).

The combination of specific ion channels with different properties expressed in various nociceptors is most likely a key determinant of their functional diversity, not only to define the class of stimuli they respond to, but also to define how they encode sensory information. As is true for any other sensory neurons, key parameters defining their functional properties include (i) the stimulus *sensitivity range*, which defines the intensity levels considered as noxious, (ii) the *sensory gain*, which defines the strength of the signal produced in response to a given change in the stimulus intensity, as well as (iii) the *response kinetic* parameters, which will alter the temporal encoding of information. Fully understanding the molecular mechanisms controlling these functional aspects requires, for each nociceptor type, comprehensive investigations to determine how an ensemble of channels orchestrates the processing of nociceptive information.

Past research has identified many ion channels involved in nociceptor functions. One of the best-studied classes of channels in pain pathways are TRP channels (Ramsey et al., 2006, Zheng, 2013). They serve as primary transduction channels for noxious temperatures (e.g., the heat-gated TRPV1 and cold-gated TRPM8), but can also act as signal amplifier within nociceptors (Geffeney et al., 2011). Many other channels have a potential or demonstrated role in the nociceptive pathway and are

considered as possible targets for pain management (Cregg et al., 2010, Raouf et al., 2010). These include Voltage-gated Calcium channels (VGCCs), Voltage-gated sodium channels, Acid-sensing ion channels (ASICs), P2X channels, as well as various Potassium channels and sodium leak channels (Park and Luo, 2010, Chizh and Illes, 2001, Du and Gamper, 2013, Wemmie et al., 2013, Wood et al., 2004). For some of them, we still have a very fragmentary vision of their role in nociceptive pathways. For instance, sodium leak channels, thought to determine the resting potential in neurons (Cochet-Bissuel et al., 2014, Lu et al., 2007), have recently been shown to play a role in second-order neurons in the afferent dorsal horn ganglion in rodents (Ford et al., 2018), but their possible function in primary nociceptive neurons is unknown.

Functional studies on mammalian nociceptors are hindered by ethical concerns, the use of anesthetics or *ex-vivo* preparations, and by the inherent biological complexity associated with the above-mentioned heterogeneity of nociceptor populations (Chen et al., 2006, Gascon and Moqrich, 2010, Woolf and Ma, 2007). A significant challenge for *in vivo* experiments regards the ability to identify a functionally homogenous population of nociceptors within and between animals. To circumvent these complications, we use here the nematode *C. elegans* as a complementary model with several advantages. First, its compact nervous system develops according to a stereotypic lineage and its connectivity was fully mapped (White et al., 1986). A specific nociceptor type can thus be reliably identified across animals. Second, the worm body is transparent, allowing non-invasive calcium imaging *in vivo* and direct optogenetic stimulation (Nagel et al., 2005). Third, a large number of mammalian genes (e.g TRPV channel genes (Glauser et al., 2011)) have functionally conserved homologs in *C. elegans*. Collectively, these features make *C. elegans* an ideal model for dissecting the molecular functions in nociceptive pathways.

C. elegans can reproduce between ~13-25°C and engage different behaviours to stay within this thermal range, such as thermotaxis and noxious heat avoidance (Hedgecock and Russell, 1975, Liu et al., 2012, Glauser, 2013). Head-targeted or whole-animal noxious heat stimulations trigger a reversal response, where worms produce transient backward locomotion (Wittenburg and Baumeister, 1999).

This response requires two thermosensory neuron pairs in the head: AFD and FLP. The AFD neurons also contribute to thermotaxis in the innocuous temperature range (Aoki and Mori, 2015, Liu et al., 2012, Goodman and Sengupta, 2018). AFD mostly responds to thermal changes when they reach a certain threshold and this response adapts relatively fast (Hawk et al., 2018). FLP neurons are polymodal nociceptors previously shown to detect high temperatures and harsh touch. Their arborized morphology also recalls that of peripheral polymodal sensory neurons in vertebrates (Hilliard et al., 2005). Optogenetic stimulation of FLP is sufficient to trigger a reversal response similar to that elicited by harsh touch and noxious heat (Schild and Glauser, 2015, Li et al., 2011). Unlike AFDs, almost nothing is known about the thermosensory function of FLPs, how they encode the heat signal, and on the molecular players required to fulfil this function.

Here, we extensively characterize temperature-evoked FLP activity using calcium imaging in intact, non-anesthetized animals. We demonstrate that FLP works as a tonic thermosensor in a surprisingly wide temperature range from 8 to 36°C, with a higher sensory gain in the noxious heat range. We highlight the functional relevance of this tonic signalling mode, which translates prolonged optogenetic FLP stimulations into sustained behavioural changes. Using genetic mutations, we also show that different ion channels control sensory gain, thermal sensitivity, and FLP response kinetics, respectively. Overall, our work establishes an effective paradigm to study the nociceptor functions *in vivo* and highlights the distribution of specific roles among many essential channels to sustain tonic signalling.

Results

Noxious heat stimuli elicit robust Ca^{2+} response in FLP

To study temperature-evoked activity in FLP, we used *[egl-46p::YC2.3]* transgenic animals expressing the YC2.3 cameleon calcium sensor in FLP (Chatzigeorgiou et al., 2010). FLP cell body calcium levels were recorded in immobilized worms whose temperature was precisely controlled thanks to a microfluidic-based device (Fig. 1A). To validate our setup, we first recorded changes in intracellular calcium concentration in response to short noxious heat stimuli (30 s at 32 °C, from a baseline at 20 °C). The calcium increases were reversible and their magnitude was remarkably constant over ~15 minutes of repeated stimulations (10 stimuli, Fig. 1B, c and d), showing no adaptation. These data indicate that worms withstand well the treatment and that FLP robustly responds to heat.

Short thermal stimuli of graded intensities trigger intracellular Ca^{2+} peaks of graded magnitudes in FLP

To better understand how FLP encodes thermal information, we first examined its temperature sensitivity window. From a 20 °C baseline, 30 s heat stimuli of increasing intensities were delivered in two-degree increments from 26 to 40 °C, with a 120 s inter-stimulus interval (ISI, Fig. 2A). The magnitude of calcium peaks in FLP increased proportionally to the thermal intensities from 26 to ~36 °C and plateaued at higher temperatures (Fig. 2C, E). We recorded a similar temperature-response relationship when using a mirror protocol with a train of stimuli of decreasing intensity from 40 to 26 °C (Fig. 2B, D, F). Blocking synaptic transmission or neuropeptide synthesis in *unc-13(e450)* or *egl-3(gk238)* mutants, respectively, left the response intact (Fig. 2G), indicating that these responses were most likely due to the cell-autonomous thermosensory activity of FLP. Furthermore, no significant YC2.3 FRET/CFP ratio change was observed in the mechanosensory CEP neurons (Fig. 2H), indicating that (i) temperature-dependent fluorescence of the YC2.3 sensor cannot account for the changes observed in FLP, and (ii) heat-evoked calcium transient is not a general phenomenon in *C. elegans* neurons, which is consistent with previous findings (Kotera et al., 2016).

The response plateau observed above 36 °C (Fig. 2B,C) in FLP could either reflect an actual plateau in calcium concentration or the saturation of the YC2.3 sensor. To address this question, we expressed a YC2.3(E31Q) mutant sensor with reduced calcium affinity and thus able to produce signal changes at higher calcium concentrations. The plateau effect was still present (Fig. S1A and B), suggesting that the FLP intracellular calcium concentration reaches a maximum and does not further increase at extreme temperatures (38-40 °C). Taken together, our data show graded FLP response intensities over a wide thermal window and indicate that the upper limit of this sensitivity window is around 36-38 °C.

Sustained thermal stimuli cause stable adjustments of intracellular Ca^{2+} levels in FLP

In principle, FLP could encode temperature changes (phasic signaling) or absolute temperature (tonic signaling). To discriminate between these two possibilities, we measured calcium levels in response to prolonged thermal stimuli (5 min). If FLP responds only to temperature changes, one would expect to see only a transient peak and a return to baseline even when temperature stays high. In contrast, if FLP responds tonically as an absolute temperature sensor, sustained calcium elevations should occur. Our data support the second model. Indeed, upon prolonged noxious heat stimulation (28, 32, or 36 °C), calcium levels increased within ~30 s to a new steady level, stayed elevated as long as the stimulus was maintained, and eventually returned to baseline when temperature returned to 20 °C (Fig. 3A). As for the magnitude of the peaks observed during short stimuli (Fig. 2C), the steady-state calcium levels grew proportionally to temperature from 28 to 36 °C (Fig. 3B).

FLP activity encodes low temperatures with a lower sensory gain as compared to noxious heat

In order to define the lower limit of FLP thermal sensitivity, we next examined the impact of thermal stimuli below the presumed *C. elegans* noxious heat range. To our surprise, calcium levels in FLP decreased in response to both short (30 s, Fig. S2A and B) and long cold stimuli (5 min, Fig. 3A blue traces) below 20 °C. We observed graded responses as a function of temperature, but the steepness of the function was reduced in the cold temperature range as compared to noxious heat range (Fig. 3B, $p<.001$ on the regression slope coefficients). To confirm that the sensitivity range of FLP is geared towards noxious heat, we also determined the impact of short heat stimuli of fixed intensity (+6°C)

from different baselines (12 to 18, 20 to 26, and 28 to 34 °C) (Fig. 3C). Consistent with a sensory gain adjusted toward noxious heat, we found that the peak amplitude increased toward the noxious heat range (Fig. 3D). In addition, we noted that the magnitude of the calcium peaks was independent of the recent thermal history (see Fig. 4A and 4B comparing a single step stimulation from 20 to 34 °C and a two-step stimulation from 20 to 28 °C and later from 28 to 34 °C).

Together, our data indicate that FLP is a tonic sensory neuron whose activity is continuously adjusted to reflect absolute temperatures over a large temperature range from 8 to 36 °C, with a higher sensory gain above 26 °C.

Steady intracellular calcium concentrations in FLP reflect current temperature independently of past growth temperature

Next, we wondered whether past growth temperature would impact FLP thermosensory activity. We thus quantified the FRET/CFP ratio produced by the YC2.3 sensor, as a correlate of absolute intracellular calcium concentration in animals grown at 15 or 25 °C. The calcium level in animals grown at 25 °C was significantly higher than that in animals grown at 15 °C (compare baselines in Fig. 4C). Furthermore, the steady calcium level reached when animals grown at 15 °C were transiently heated to 25 °C was similar to that in animals that had been always maintained at 25 °C (Fig. 4C and D). The mirror situation was observed when animals grown at 25 °C were transiently cooled to 15°C. Collectively, our data suggest that FLP may serve as an absolute thermometer encoding temperature irrespective of growth thermal history.

The TRPV channel genes *osm-9* and *ocr-2* are required for FLP activity

To identify molecular components involved in generating the heat-evoked response in FLP, we analyzed the impact of mutations in the genes of several candidate channels. The TRPV channel subunits OSM-9 and OCR-2 are candidate thermoreceptors in *C. elegans* and null mutations in *osm-9* and *ocr-2* genes synergize to reduce noxious heat avoidance, while not fully abolishing it (Glauser et al., 2011). Previous studies showed that *osm-9* is partially required for heat-evoked calcium transient

in FLP (Liu et al., 2012, Chatzigeorgiou and Schafer, 2011), but whether it controls FLP thermal sensitivity or its sensory gain is unknown.

We started by evaluating the impact of TRPV channel mutations on the thermal sensitivity of FLP. Knocking out *osm-9* reduced FLP calcium responses, with a markedly right-shifted temperature-response curve as compared to wild type when assessed with short stimuli of graded intensity (Fig. 5A, left). The response did not reach the same level as in wild type, nor reached a plateau at temperature as high as 40 °C (the highest temperature in our setup). The maximal slope of the temperature-response relationship was not significantly reduced in *osm-9* as compared to wild type (Fig. S3A). The right shift in the temperature-response curve was also clearly maintained when the data were normalized to the maximal response (Fig. S3B). Collectively, these analyses suggest a significant shift in sensitivity in animals lacking functional OSM-9. Knocking out *ocr-2* produced a small but significant reduction in the FLP calcium response ($p<.001$, Fig.5A, middle). Knocking out both *osm-9* and *ocr-2* produced a further decrease in FLP response as compared to knocking out only *osm-9* (Fig. 5A right, S4A and B). The additive impact of the two mutations was confirmed by a two-way ANOVA (with *osm-9 allele* and *ocr-2 allele* as factors) showing significant main effects ($p<.001$ for each factor), but no interaction effect ($p=.55$). The remaining FLP response at high temperature in the double mutant suggest the existence of additional, unidentified thermoreceptor molecules required for the response to extreme noxious temperatures (>32°C).

We next examined the impact of TRPV channel mutations on FLP sustained calcium elevation in response to prolonged (5 min) heat stimuli at 32°C. We found that single as well as double mutants were still able to produce long-lasting calcium elevations (Fig. 5B), even if the magnitude of the steady calcium changes varied across genotypes. These variations were consistent with the results of the sensitivity analysis (Fig. 5A), with the single *ocr-2* mutation producing a small reduction, the single *osm-9* mutation an intermediate reduction, and the double *osm-9 ocr-2* mutation a strong reduction (Fig. 5B and S4C and D).

Collectively, our *osm-9* and *ocr-2* mutant analyses suggest that these two TRPV channels are required for normal thermal sensitivity in FLP, but not needed for maintaining stable, tonic calcium elevation upon sustained heat stimulation.

Specific VGCCs are required to maintain FLP sensory gain and thermal sensitivity

VGCCs are major actors in the control of calcium influx from the extracellular space and play multiple roles from signal amplification and transmission to vesicle exocytosis (Bachnoff et al., 2013). The *C. elegans* genome contains single genes encoding each of three VGCC pore-forming subunit classes: *egl-19* (L-type), *unc-2* (N-type) and *cca-1* (T-type) (Hobert, 2013). To evaluate the contribution of these channels to heat-evoked FLP calcium signals, we quantified relative calcium changes in response to short and sustained stimuli in reduction-of-function mutant *egl-19(n582*) and loss-of-function mutants: *unc-2(ra612)* and *cca-1(ad1650)*. We found that the mutations in *egl-19* and *unc-2* significantly impaired heat-evoked calcium responses, while that in *cca-1* had no or markedly lower effects.

Mutation of *unc-2* produced effects relatively similar to those of *osm-9*. In response to short stimuli, *unc-2* mutants had a right-shifted temperature-response curve and its maximal slope was not significantly lower than that of the wild type (Fig.5C left and S3A). Even when peak amplitude was normalized and expressed as a percentage of the maximal changes, the response curves between wild type and *unc-2* were very distinct (Fig. S3B). These results suggest a selective role of UNC-2 in supporting FLP thermal sensitivity to low range noxious temperature. The magnitude of the calcium elevation upon prolonged stimulation at 32 °C was lower in *unc-2* mutants than in wild type, but persisted as long as the stimulus was maintained (Fig.5D, left).

Like for *unc*-2, mutation of *egl-19* produced a marked decrease in calcium changes upon short stimulations of gradual intensities (Fig. 5C, middle). However, the shape of the temperature-response curve was differently affected. The curve flattens at high temperatures and its maximal slope is decreased compared to that of the wild type (Fig. 5C, middle and S3A). When the response amplitude was normalized and expressed as a percentage of the maximal response, the *egl-19* and wild type

curves were very similar (Fig. S3B). These changes are consistent with a model in which EGL-19 does not directly influence thermal sensitivity, but mostly contributes to amplifying the Ca^{2+} response and maintaining the general sensory gain. Upon prolonged stimulation at 32°C, the magnitude of the calcium elevation was lower in *egl-19* mutants than in wild type, but persisted throughout the duration of the stimulus (Fig. 5D, middle).

Collectively, these results highlight that VGCCs control heat-evoked intracellular calcium activity in FLP and suggest (i) that N-type channels are particularly important for thermal sensitivity, (ii) that L-type channels contribute to maintain a high sensory gain, but (iii) that neither channel types is required to maintain stable calcium signaling upon long-term stimulation.

UNC-77/NCA-1 and NCA-2 sodium leak channels control FLP calcium signaling

Sodium leak channels (NALCNs) regulate crucial neural processes such as the propagation of neuronal excitation and the accuracy of synaptic transmission (Jospin et al., 2007, Lu et al., 2007, Yeh et al., 2008). Their role in ascending nociceptive transmission has been recently highlighted in the central pain pathway (Ford et al., 2018), but their potential role in primary nociceptors is unknown. To address their role in FLP, we examined the impact of mutations in the two *C. elegans* NALCN genes *unc-77* (also named *nca-1*) and *nca-2*. Our data show that mutations in either NALCN gene reduced the magnitude of heat-evoked calcium changes, both during short and prolonged stimulations (Fig. 5E and g). A right-shifted temperature-response curve (Fig. 5E, left, and S3B), but unaltered maximal slope (Fig. S3A) suggest that the *unc-77* mutation affects thermal sensitivity, similarly to *osm-9*. The defect in *nca-2* combined a right-shifted curve (Fig. 5E, right, and S3B) and a reduced maximal slope (Fig. S3A), suggesting a broader impact on thermal sensitivity and sensory gain. Neither mutation affected the ability of FLP to maintain steady-state calcium elevation upon prolonged stimulation (Fig. 5G). Interestingly, the off-rate kinetics upon stimuli termination was significantly slower in *nca-2* mutants (Fig. S5A and B).

Collectively, our data suggest that UNC-77 controls FLP thermal sensitivity, whereas NCA-2 plays a role in thermal sensitivity, sensory gain maintenance and signal kinetics during thermal stimuli termination.

UNC-68/ryanodine receptor channels are necessary to maintain calcium signals upon prolonged stimulations

Ryanodine receptors are Ca^{2+} channels expressed in the membrane of the endoplasmic reticulum (ER) that can couple cell excitation with Ca^{2+} release from intracellular stores. Because the sole *C. elegans* Ryanodine receptor ortholog, UNC-68, was previously shown to function in tonic sensory neurons (Busch et al., 2012), we evaluated the impact of the *unc-68(r1161)* null mutation on heat-evoked calcium responses in FLP. No significant difference was observed with wild type for short stimulations of graded intensities in the 26-40 °C range, indicating intact thermal sensitivity and sensory gain for transient stimulations (Fig. 5F). Upon prolonged stimulations, however, we noticed a larger variability in the response and a gradual decrease in calcium level after the first minute of stimulation (Fig. 5H). Our results show that UNC-68 channels are dispensable for Ca^{2+} responses to short stimuli, but are necessary to produce sustained and stable Ca^{2+} elevation upon prolonged thermal stimulations.

Impact of mutations on noxious heat-evoked reversal

Next, we wanted to determine if the mutations altering FLP calcium responses would also impair the noxious heat-evoked reversals. The role of TRPV channel genes was demonstrated previously (Glauser et al., 2011), but that of VGCCs, sodium leak channels, and Ryanodine receptor genes is unknown. Therefore, we compared heat-evoked reversal responses in N2 wild type and *unc-2*, *egl-19, cca-1, unc-77, nca-2* and *unc-68* mutants. Wild type animals exposed to a 4 s heat pulse delivered with infrared lamps produced a strong, transient increase in reversal rate (Fig. S6A). Consistent with the mutations' impact on heat-evoked calcium activity in FLP, the frequency of these heat-evoked reversals was significantly reduced in *unc-2*, *egl-19, unc-77* and *nca-2*, but not in *cca-1* and only marginally in the *unc-68* mutants (Fig. S6B).

Because the *nca-2* mutation slowed down the kinetics of calcium decrease in FLP upon stimulus cessation (Fig. S5), we hypothesized that *nca-2* mutants may present a delayed decrease in reversal rate in the post-stimulus period. We thus compared the kinetics of the reversal decay period in wild type and *nca-2* mutants (Fig. S6C). The reversal rate decay in the post-stimulus period was significantly delayed in *nca-2* mutants, confirming our hypothesis.

Tonic FLP activation produces UNC-68-dependent sustained behavioral changes

The ability of FLP to produce sustained activity upon prolonged stimulation (Fig. 3 and 4) suggests it might also have long-term behavioral impact. To explore this aspect, we submitted animals to prolonged, 5 min optogenetic FLP stimulations and analyzed reversal and speed responses. Our data highlight a phasic reversal response and a tonic speed response, that were fully dependent on the presence of all-*trans*-retinal (ATR) in the growth media (Fig. S7A and B). Indeed, in the presence of ATR, the reversal rate markedly increased in the first minute, but rapidly returned to baseline for the rest of the stimulation period (Fig. 6A). In contrast, locomotory speed rose, remained significantly higher than baseline until the stimulus termination and thereafter returned to baseline (Fig. 6B). During the sustained stimulation, a slow decay in speed was observed, which could reflect opsin fatigue or response adaptation taking place downstream of FLP activation. Shorter stimuli of 1 or 3 min produced similar speed elevations, the duration of which was commensurate to that of the stimuli (Fig. 6C and D). Furthermore, stimulations of graded light intensities produced a graded impact on speed (Fig. 6E).

Finally, we wanted to evaluate if the *unc-68* mutant inability to sustain FLP calcium response to prolonged stimulation (Fig. 5H) would be associated with an impaired sustained speed response. Because baseline speed is strongly decreased in *unc-68(r1161)* animals, which complicates comparison interpretation, we used a *unc-68(r1161);[myo-3p::unc-68]* transgenic line in which *unc-68* expression is rescued in body wall muscle, substantially restoring locomotion. Consistent with a role of UNC-68 in maintaining tonic FLP activity, the loss of *unc-68* in non-muscular tissues did not reduce the initial increase in locomotory speed evoked by sustained optogenetics FLP activation, but

the elevated speed decayed significantly faster than in control animals, returning to baseline speed while the stimulus was still applied (Fig. 6F). Collectively, these data reveal a phasic reversal response and an *unc-68*-dependent tonic speed elevation in response to persistent FLP activation.

Discussion

Comprehensively understanding the functions of nociceptor neurons is an essential step towards elucidating how animals can produce protective behaviors, as well as in guiding biomedical research toward better pain management. Our work establishes FLP neurons in *C. elegans* as a fruitful experimental model to study the molecular and cellular mechanisms mediating thermo-nociceptive functions *in vivo* in intact animals. Our data show that FLP is a tonic sensory neuron that non-linearly encodes absolute temperatures within an unexpectedly wide thermal window and that prolonged FLP activity results in sustained behavioral changes. Furthermore, our genetic analysis identifies several specific ion channels required to maintain different characteristics of FLP functions such as thermal sensitivity, sensory gain, and signal stability, which are essential for proper noxious heat avoidance.

FLP thermal sensitivity window

The upper FLP sensitivity limit around 36-38 °C appears to be adjusted to worm physiology. Indeed, crawling worms rapidly paralyze when exposed to temperatures above 38 °C (Schild and Glauser unpublished observations). Therefore, it would probably be unnecessary for the worm to develop the ability to discriminate temperatures in this extreme thermal range, as no protective behavior could be executed. The particularly steep temperature-activity relationship from 26 to ~36 °C appears globally consistent with several previous observations on noxious heat-evoked behaviors (Schild and Glauser, 2013, Mohammadi et al., 2013, Glauser et al., 2011). Unexpectedly, we found that FLP encodes thermal information outside of the noxious heat range, toward temperatures as cold as 8°C. When tested with a baseline calcium level at 20°C (growth temperature), the FLP cold response was a calcium decrease. This is the opposite response as that observed in the PVD cold-thermosensor, which produced calcium elevations in response to cold stimuli of similar amplitudes (Chatzigeorgiou et al., 2010). This latter observation in PVD, the lack of signal change in CEP neurons, together with the marked decrease in FLP signal change in some mutants, constitutes an important validation point for our method. Indeed, it highlights that the large temperature-evoked YC2.3 Cameleon signal changes in FLP cannot be due to intrinsic thermo-dependent properties of the sensor. Whether the reduction of

FLP activity at low temperatures is *per se* a signal serving any significant function, including cold-avoidance, remains undetermined. Nevertheless, the ability of FLP neurons to encode thermal information from noxious cold to noxious heat is noteworthy, as temperature sensation in these different ranges are usually performed by different types of thermoreceptor neurons in mammals (Vriens et al., 2014).

FLPs are tonic thermosensory neurons

One of our main findings is that FLP acts as a tonic sensor, encoding the absolute temperature level as a steady-state calcium level, rather than encoding temperature changes. FLP behaves very differently from the extensively characterized thermosensor AFD. AFD produces rapid and significant increases in calcium when the temperature reaches a certain threshold, which could vary according to past thermal experience (Goodman and Sengupta, 2018, Chung et al., 2006, Clark et al., 2006). The AFD calcium response can adapt relatively fast (less than a minute) upon sustained thermal change and mainly encodes the rate of change rather than the intensity of the stimulus (Hawk et al., 2018). In contrast, we found no evidence of adaptation in the FLP response during 5 min of sustained stimulation, during 15 min of repeated pulse stimuli, or when animals were cultivated at different temperatures. This absence of sensory adaptation in FLP is compatible with a dual role as nociceptor and as ‘absolute thermometer’.

Our behavioral analysis shows that upon optogenetic FLP activation, animals produce a rapid increase in reversal rate, which is in line with several previous studies (Liu et al., 2012, Mohammadi et al., 2013, Schild and Glauser, 2015). In addition, using persistent stimulation protocols, we are now showing that this effect is transient and followed by a more sustained behavioral state, in which animals maintain a higher speed as long as FLP activity persists. This situation is analogous to the speed control by oxygen-sensing neurons, including the requirement for *unc-68* (Busch et al., 2012). The recruitment of calcium from intracellular store might be a general mechanism enabling sustained activity in tonic sensory neurons.

Task allocations among ion channels to maintain proper FLP functioning

Our genetic analysis suggests that specific calcium signaling features in FLP are under the control of genetically distinct molecular pathways and highlight specific ion channel functions. One of the main limitations of our analysis, however, is that the use of mutants entails a permanent defect in the whole animal. Therefore, we cannot presently discriminate between the acute impact of channel loss and the chronic impact that possibly involves more complex changes and compensatory mechanisms; neither can we assume that these channels function cell-autonomously in FLP. However, since the FLP calcium response is intact in mutants with impaired synaptic communication and neuropeptide synthesis, it is probable that the channels examined here function at least in part by directly regulating FLP physiology. Although more complex genetic manipulations will be required to address the exact locus of action of each channel, we propose here a working model on how these channels may control the different features of FLP signal processing (see Fig. 7 and next paragraphs).

The first feature regards the thermal sensitivity range. Our data suggest that the TRPV channel OSM-9, the N-type VGCC UNC-2, as well as the sodium leak channels UNC-77 and NCA-2 have a specific contribution to maintaining the calcium response in the lower range of noxious temperatures (<~32°C). As a TRPV1 channel homolog, OSM-9 is a candidate thermoreceptor molecule (Glauser et al., 2011, Liu et al., 2012, Chatzigeorgiou and Schafer, 2011). The thermal threshold of OSM-9 could potentially fall within this range and one or more unidentified thermosensory channels could respond to higher temperatures. The specific implication of UNC-2, UNC-77, and NCA-2 in maintaining the response in the low range of noxious temperatures is more surprising, because there is, to our knowledge, no evidence that they can serve as thermoreceptor molecules. One possible explanation could be that these channels functionally interact with OSM-9, while they would not interact with a thermosensor active at higher temperatures. Additional studies will be needed to address the nature of these channel contributions.

The second feature regards sensory gain, which was reduced in *egl-19* and *nca-2* mutants. L-type VGCCs have already been linked to signal amplification in different neurons (Dixon et al., 2012). In

FLP, the L-type VGCC EGL-19 may function similarly and increase the calcium influx triggered by initial heat-induced membrane depolarization. The loss of NCA-2 sodium leak channels may cause a general decrease in cell excitability by affecting the constitutive membrane properties and causing a hyperpolarization.

The third feature regards signal kinetics. Our data suggest that NCA-2 is required for the rapid termination of calcium signaling in FLP. The simplest explanatory mechanism would imply that the post-stimulus repolarization in FLP depends on passive cation efflux through leak channels and that this process slows down in the absence of functional NCA-2 channels, due to the reduced cation conductance. As proposed in Fig. 7, additional channels are most likely to be involved in signal termination, such as potassium channels, whose functions are highly conserved (Salkoff et al., 2005). Another striking finding about calcium kinetics is the requirement of the Ryanodine receptor UNC-68 to maintain calcium elevation and behavior changes upon prolonged stimulation, but not for acute responses to sudden changes. We propose that the initial calcium response upon heat stimulation mainly relies on extracellular calcium stores and a series of channels at the plasma membrane, but that the prolonged response relies on intracellular stores in order to maintain a tonic-signaling regime (Fig. 7). The UNC-68-dependent response might be due to Calcium-Induced-Calcium-Release (Roderick et al., 2003) (CICR), which first requires calcium entry from extracellular stores.

Conclusion

In mammals, it has long been recognized that phasic and tonic nociceptors co-exist in the heterogeneous pool of nociceptors. However, we know very little about the molecular machinery that controls their signaling mode and on how these different modes govern sensory perception and behavior. Our study sheds light on the molecular players controlling essential aspects of a genetically identified *C. elegans* thermonociceptor and highlights the functional implication of tonic signaling in shaping aversive behaviors. Given the high conservation of neuronal functions across animals, the result of the present and future studies with this fruitful experimental paradigm may provide useful insight into the function of ascending nociceptive pathways.

Acknowledgments

We are grateful to Lisa Schild and Laurence Bulliard for expert technical support, to Marc Hammarlund, Piali Sengupta and Bill Schafer for the gift of material and to Boris Egger from the Bioimage facility (Departments of Biology and Medicine, University of Fribourg) for assistance with microscopy. Some strains were provided by the CGC, which is funded by NIH Office of Research Infrastructure Programs (P40 OD010440). The study was supported by the Swiss National Science Foundation (BSSGI0_155764 and PP00P3_150681 to DAG), by the Medical Research Council and Wellcome Trust (MR/N004574/1 and 109614/Z/15/Z to KEB) and by the Royal Society (RG140332, to KEB), as well as a BMBS COST Action (BM1408).

Author Contributions

Conceptualization, D.A.G.; Methodology, D.A.G., G.S., A.-S.L., and K.E.B.; Formal Analysis, D.A.G., G.S. and A.-S.L.; Investigation, G.S., A.-S.L., S.T.; Resources, G.S., A.-S.L. and F.M.; Writing – Original Draft, D.A.G. and G.S.; Writing – Review & Editing, D.A.G., G.S. and K.E.B.; Supervision, D.A.G.; Funding Acquisition, D.A.G.

Declaration of Interests

The authors declare no competing interests.

Figure titles and legends

Figure 1: FLP nociceptor responds to noxious heat.

(**A**) Schematic of the thermal microfluidic device mounted on an agarose pad with glued worm (top). Picture of the system as assembled on an epifluorescence microscope (middle). Picture of a worm head, arrow indicates FLP soma (bottom), scale bar 20 µm.

(**B**) Illustration of a heat stimulation protocol with ten stimuli.

(**C**) FLP cell body calcium response the protocol in **B** and isothermal control at 20°C. Average $\Delta R/R_0$ as solid lines and SEM as coloured shades.

(**D**) Heat map reporting the individual animal responses averaged in **C**.

Figure 2: Calcium increase in FLP is proportional to the thermal stimulus intensity.

(**A**, **B**) Stimulation protocols with successive 30 s heat stimuli of increasing/decreasing intensities between 26 and 40°C and inter-stimulus intervals (ISI) of 120 s.

(**C**, **D**) FLP cell body calcium response in *[egl-46p::YC2.3]* animals with average $\Delta R/R_0$ as solid lines and SEM as grey shades. Heat map reporting the response of individual animals

(**E**) Peak comparison from data in **C**. Dots: average, error bars: SEM. *, $p<.01$ by Bonferroni contrasts. ns, not significant.

(**F**) Peak comparison between data in panels **C** and **D**, showing no significant difference by two-way ANOVA and contrasts at every temperature (ns). Dots: average, error bars: SEM. $n\geq8$.

(**G**) Heat-evoked FLP cell body calcium response in wild type, *unc-13(e450)* and *egl-3(gk238)* animals stimulated as described in **A**, showing no significant difference by two-way ANOVA and contrasts at every temperature (ns). Dots: average, error bars: SEM. $n\geq8$.

(**H**) Heat-evoked calcium response in FLP and CEP cell bodies in *[egl-46p::YC2.3]* and *[dat-1p::YC2.3]* animals, respectively, stimulated with stimuli of increasing intensities between 26 and 40°C and showing no significant response in CEP. Lines: average $\Delta R/R_0$; shadows: SEM; $n\geq11$ animals.

See also Figure S1.

Figure 3: FLP nociceptors respond to absolute temperature.

(**A**) FLP cell body calcium responses to sustained stimulation (5 min) at the indicated temperature, from a baseline at 20°C (30 first seconds) followed by a return to baseline temperature. Solid lines indicate averages and coloured shades are SEM.

(**B**) Temperature-response curves from data in panel **A**, considering the $\Delta R/R_0$ steady-state value averaged between $t=120$ and $t=300$ s for each animal. Dots are average values across independent animal traces with error bars being SEM. *, $p<.05$ and **, $p<.01$ by Bonferroni contrasts with

adjacent data points. Two linear regression curves (dotted lines) in the hot and cold ranges have a significantly different slope ($p<.0001$).

(**C**) Six degrees Celsius upstep experiments from different baseline temperatures. Data (bottom) plotted as in panel **A**, with line colours matching that in the protocol schemes (top).

(**D**) $\Delta R/R_0$ peak amplitudes from data in **C**. Significant protocol impact by one-way ANOVA. * $p<.05$ and **, $p<.01$ by Bonferroni contrasts.

See also Figure S2.

Figure 4. Absence of short and long term adaptation in FLP

(**A**, **B**) Calcium level changes in FLP cell bodies of *[egl-46p:.YC2.3]* animals quantified with two protocols as schematically depicted: direct stimulation at 34°C from a 20°C baseline versus indirect stimulation to 34°C with an intermediate step at 28°C. (**A**) Average calcium traces (lines) with SEM as grey shades. $n\geq6$ animals. (**B**) Peak quantification at 34°C. ns, not significant by Student's *t*-test.

(**C**, **D**) Calcium levels in FLP cell bodies of *[egl-46p:.YC2.3]* animals grown either at 15 or 25°C and submitted to a temperature increase to 25°C or decrease to 15°C, respectively. (**C**) Average calcium traces (blue and red lines) with SEM as lighter shades. $n\geq6$ animals. (**D**) Quantification of the calcium levels at baseline and during the stimulus, error bars represent SEM. Two-way ANOVA showed no significant effect of *growth temperature*, but only of *current temperature*. *, $p<.01$; ns, not significant by Bonferroni posthoc tests.

Figure 5: Noxious heat-evoked FLP calcium responses in ion channel mutants.

(**A**, **C**, **E**, **F**) Heat-evoked calcium peaks in FLP cell bodies as a function of stimulus intensity in wild type and mutants for candidate channels. TRPVs: *osm-9(ky10)*, *ocr-2(ak47)*, *osm-9(ky10) ocr-2(ak47)*; N-type VGCC: *unc-2(ra612)*; L-type VGCC: *egl-19(n582)*, T-type VGCC: *cca-1(ad1650)*; NALCNs: *unc-77(gk9)*, *nca-2(gk5)*; RYR: *unc-68(r1161)*. Each dot represents the average $\Delta R/R_0$ peak amplitude reached upon 30 s stimuli from a baseline at 20 °C with an ISI of 60 s (as in Figure 2H), with SEM as error bars. Dotted lines indicate 4-parameter sigmoid curve fittings. $n\geq10$ independent recordings each in a different animal. *$p<.05$ and **, $p<.01$ versus wild type by Tukey tests.

(**B**, **D**, **G**, **H**) Heat-evoked tonic calcium responses in FLP cell bodies in wild type and indicated mutants. Solid lines indicate the averages, grey shades indicate the SEM, $n\geq10$ independent recordings each in a different animal. Red shades indicate the 5 minute stimulation period at 32 °C from a baseline at 20 °C.

See also Figures S3, S4, S5 and S6.

Figure 6. Behavioral response to sustained FLP optogenetic stimulation.

(**A, B**) Reversal and speed response in *domIs355[FLP::CoChR]* animals left in the dark (-light) or exposed for 5 minutes with 15 W/m^2 of blue light (+light). (**C**, **D**) Comparison of the speed response as in **B** with light stimuli lasting 5, 3, and 1 min.

(**E**) Speed increase over pre-stimulus baseline as a function of light intensity; speed averaged over a 5 min stimuli window. (**F**) Comparison of FLP-evoked 5 min tonic speed elevations between wild type and *unc-68(r1161)* null mutant animals carrying a muscle-specific *unc-68* rescue transgene.

All data as average (lines or dots) and SEM (shades or error bars) of $n>5$ independent plate recordings, each tracking at least 50 animals. For statistical comparisons, the time courses were divided into 30 s epochs and average values calculated for each epoch. Tukey's multiple comparison tests were used to compare conditions for each epoch.*, $p<.01$ versus no light control; #, $p<.05$ and ##, $p<.01$ versus wild type.

See also Figure S7.

Figure 7. Hypothetical model of ion channel functions in FLP.

FLP response to heat is divided into four steps (grey boxes) and each step is linked to specific functional properties (green boxes). FLP presumably detects noxious thermal stimuli via OSM-9 and OCR-2, as well as at least one additional type of unidentified thermosensor. OSM-9 and OCR-2 could also function as amplifiers of the signal coming from other thermosensors during the detection phase. UNC-77, UNC-2 and NCA-2 participate to confer high thermal sensitivity. UNC-77 and NCA-2 are proposed to function by adjusting the resting membrane potential, possibly by setting the overall membrane permeability for sodium. UNC-2 is proposed to promote depolarization-induced Ca^{2+} entry. The signal amplification depends on EGL-19 which, together with NCA-2, is required to maintain a high sensory gain. Increased cytoplasmic Ca^{2+} might activate the Ryanodine receptor RyR/UNC-68 at the endoplasmic reticulum (ER) membrane by Calcium-Induced Calcium Release (CICR). UNC-68 opening induces Ca^{2+} release from the ER, reinforcing the effect of the initial stimulus and enabling the generation of stable, sustained FLP activation. When stimulation ends, prompt termination of the signal requires NCA-2, possibly controlling the repolarization kinetics by setting the maximal flow of cations. K^+ channels (not studied in the present work) are also included, as they are very likely to influence the neuron physiology, notably during the termination phase.

STAR Methods

LEAD CONTACT AND MATERIALS AVAILABILITY

All new strains and plasmids created in this study will be provided on request. Further information and requests for resources and reagents should be directed to and will be fulfilled by the Lead Contact, Dominique Glauser (dominique.glauser@unifr.ch).

EXPERIMENTAL MODEL AND SUBJECT DETAILS

C. elegans strains were maintained according to standard techniques on nematode growth medium (NGM) agar plates seeded with OP50. On the first day, adult hermaphrodytes were analyzed.

METHOD DETAILS

Molecular cloning

dg229 *[slot1 Entry QUAS promoter]* and **dg240** *[slot2 Entry QF]* have been previously described (Schild et al., 2014).

pMH473 *[slot3 Entry unc-54 3'UTR]* was a gift from Marc Hammarlund.

dg69 *[slot1 Entry egl-46 promoter]* was produced by BP recombination between pDONR_221 (Invitrogen) and the product of a PCR amplifying genomic DNA with egl-46pF and egl-46pR primers.

dg718 *[slot2 Entry YC2.3]* was produced by first amplifying the YC2.3 sequence by PCR from the plasmid *nmr-1p::YC2.3* (gift from Bill Schafer's lab) with YC2.3AttB1 and YC2.3AttB2 primers, which contained attB1 and attB2 recombination sites, respectively. The PCR product was recombined with pDONR_221 in a BP reaction.

dg719 *[slot2 Entry YC2.3(E31Q)]*, carrying the low-affinity calcium sensor YC2.3(E31Q), was generated by site-directed mutagenesis on dg718. A PCR reaction was performed with dg718 as template using E31QF and E31QR primers. The PCR product, consisting of an open version of the whole plasmid, was then circularized by ligation with the DNA Ligation Kit, Mighty Mix (Takara ®). In the E31QF primer, the first nucleotide corresponds to the mutated nucleotide introducing the E31Q mutation into the Calmodulin coding sequence within the YC2.3 sensor.

dg277 *[egl-46p::QF::unc-54-3'UTR]* was created by LR recombination between dg69, dg240, pMH473 and pDEST-R4-P3.

dg720 *[QUAS::YC2.3(E31Q)::unc-54-3'UTR]* was created by LR recombination between dg229, dg719, pMH473 and pDEST-R4-P3.

Transgenesis

Transgenic animals expressing the YC2.3(E31Q) sensor were created by gonad micro-injection (Evans, 2006) of the following DNA mix: dg277 *[egl-46p::QF]* (20 ng/µl) + dg720*[QUAS::YC2.3(E31Q)::unc-54-3'UTR]* (20 ng/µl) + coel::RFP *[unc-122p::RFP]* (20 ng/µl). *coel::RFP* (*unc-122p:.RFP*) was a gift from Piali Sengupta (Addgene plasmid # 8938).

Animal preparation for heat-evoked calcium activity imaging

0.3 mm-thick agarose pads were prepared with 2% agarose in M9 buffer (KH_2PO_4 22 mM, Na_2HPO_4 22 mM, NaCl 85 mM, $MgSO_4$ 1 mM) using glass coverslips as support, as previously described (Girard et al., 2007). Transgenic fluorescent animals expressing the Cameleon sensor in their FLP neurons were pre-selected by using an epifluorescence stereomicroscope at least one hour prior to the experiment. For each recording, one worm was picked with an eyelash pick and transferred to an agarose pad. Worms were immobilized by applying Dermabond surgical glue (Closure Medical), using glass capillary needles operated by mouth. The glue was initially applied close to the tail of the worm, on its dorsal side (keeping the ventral side free of glue in order to allow intact egg-laying physiology) and then along the whole body, close to the head but without glueing the nose. With this procedure, the worm was able to sense environmental cues and remained alive throughout the recording. After glue polymerization (around 30 s), M9 buffer was added close to the worm to keep the environment slightly humid and prevent exsiccation of the agarose pads. A plastic spacer was placed on the coverslip (Fig.1A, shown in light red) between the worm and the microfluidic chip. This preparation was mounted in the Cherry Temp (Cherry Biotech, Rennes, France) microfluidic chamber system. With this system, sample temperature can be stably maintained (variations < 0.1 °C) or quickly changed to a new steady temperature (within 10 s), thanks to a circuit switch between two pre-

equilibrated Peltier elements located near the sample. The temperature of the microfluidic chamber was preset to 20°C to maintain a constant baseline temperature before initializing the experimental protocols. Experiments with baseline at 20°C were performed in a temperature-controlled environment constantly set at 21-22°C in order to prevent worm from undergoing significant habituation during sample preparation. The worm glueing protocol had an average duration of 2-3 minutes per worm and the preparation was suitable for imaging for a maximum of 30 min under healthy conditions.

Calcium imaging

Adult worms were imaged using an inverted epifluorescence microscope (Leica DMI6000B) with a HCX PL Fluotar L40x/0.60 CORR dry objective, a Leica DFC360FX CCD camera (1.4M pixels, 20 fps), an EL6000 Light Source, and equipped with fast filter wheels for FRET imaging. Excitation filters for CFP and FRET: 427 nm (BP 427/10). Emission filters for CFP: 472 (BP 472/30) and for FRET: 542 nm (BP 542/27). Dichroic mirror: RCY 440/520. At least one minute of initial recording at 20°C was used as baseline. Depending on the duration of the thermal stimulation protocol, different acquisition rates were used, in order to have enough details in the acquisition and limit photobleaching and phototoxicity. For long recordings (more than 15 minutes), the acquisition rate was of one frame every 2 seconds (0.5Hz). For short recordings, such as tonic response protocols (lasting for 7 minutes or less), one frame per second (1Hz) was used.

Optogenetics behavioral assays

Adult worms were bleached according to standard protocols and eggs left to grow for 62-64 hours at 20 °C in order to obtain synchronized adults. All-*trans* retinal (ATR) was added to the medium as previously described (Schild and Glauser, 2015). On the day of the experiment, these synchronized worms were collected with distilled water, transferred in 1.5 ml tubes, and washed three times in order to remove bacterial food. During washes, worms were let to settle by gravity to the bottom of the tube. About 70 to 140 worms were plated onto unseeded NGM plates. Animals were left to acclimate for

one hour at room temperature (23 +/- 0.5 °C) and spread homogeneously onto the plate before the start of the behavioral assay.

Homogenous blue light stimuli were delivered obliquely though a ring of blue LED (460 +/- 10 nm). Power was adjusted with an optocoupler-based system and the delivered light intensity was empirically determined with a portable spectrophotometer (USB4000, OceanOptics). Movies of crawling worms (50 to 100, per plates) were recorded with a DMK23UP1300 camera (The Imaging Source, Germany). The Multi Worm Tracker (Swierczek et al., 2011) software was used to track worms and determine their speed, and a custom-written software was used to flag reversal events, similar to the analyses performed in a previous study (Schild and Glauser, 2013).

Heat stimulation for behavioral analysis

Heat stimuli were delivered with four 100 W infrared lamps projecting light obliquely on 6-cm Petri dishes deposited on a temperature-controlled aluminum plate. The induced temperature change was ~1.4°C/s (from 22°C to 28°C) as measured with a thermal probe maintained at the top of the agar surface. Movies were recorded and reversal events quantified as described above for the optogenetic analysis.

QUANTIFICATION AND STATISTICAL ANALYSIS

Calcium imaging analysis

All time-lapse recordings were analyzed using LAS X software (Leica). To calculate the FRET ratio, we selected a first region of interest (ROI), delimiting the background, and a second ROI, which included FLP soma for CFP and FRET channels. For each channel, the $ROI_{background}$ values were subtracted from the ROI_{FLP} values. The resulting values for FRET and CFP respectively (namely $FRET_{FLP\text{-}background}$ and $CFP_{FLP\text{-}background}$) were divided and the FRET ratio (FRET/CFP) was calculated as follows:

$$R = FRET\ ratio\ = \frac{FRET_{FLP-background}}{CFP_{FLP-background}}$$

For baseline normalization, the FRET ratio R was expressed as a $\Delta R/R_0$, where ΔR is R- R_0 and R_0 is the average of R over the last 30 s prior to stimulus onset.

Curve fitting and statistics

Curve fitting for temperature-response relationships was performed on the online platform *zunzun.com* (http://zunzun.com), using linear regression or 4-parameter sigmoids. To determine if regression coefficients between different curves were statistically different, we used the method presented by Paternoster and colleagues (Paternoster et al., 1998). Student's *t*-tests were used for comparisons involving two conditions and ANOVAs for comparisons involving more than two conditions.

DATA AND CODE AVAILABILITY

This study did not generate/analyze datasets/code.

KEY RESOURCES TABLE

REAGENT or RESOURCE	SOURCE	IDENTIFIER
Chemicals, Peptides, and Recombinant Proteins		
Dermabond surgical glue	Closure Medical	Art. No 129463
Experimental Models: Organisms/Strains		
C. elegans:AQ2145 *ljEx19[egl-46p::YC2.3; lin15(+)]*	Gift from Bill Schafer (Chatzigeorgiou et al., 2010)	N/A
C. elegans: *AQ912 lin-15(n765ts); ljEx51[dat-1p::YC2.3+lin-15]*	Gift from Bill Schafer	N/A
C. elegans: TR2170 *unc-68(r1161)V*	CGC	N/A
C. elegans: ZM2960 *nca-2(gk5) III; unc-77(gk9) IV*	CGC	N/A
C. elegans: JD21 *cca-1(ad1650) X*	CGC	N/A
C. elegans: MT1212 *egl-19(n582) IV*	CGC	N/A
C. elegans: LX748 *ocr-2(ak47) IV; osm-9(ky10) IV*	CGC	N/A
C. elegans: CX4544 *ocr-2(ak47) IV*	CGC	N/A
C. elegans: CX10 *osm-9(ky10) IV*	CGC	N/A
C. elegans: DM612 *unc-2(ra612) X*	CGC	N/A
C. elegans: *VC461 egl-3(gk238) V*	CGC	N/A
C. elegans: *CB450 unc-13(e450) che-3(ky1018) I*	CGC	N/A
C. elegans: *DAG356 domIs355[mec-3p::QF, mec-4p::QS, QUAS::CoCHR, unc122p::RFP]*	(Schild and Glauser, 2015)	N/A
C. elegans: *DAG680 unc-68(r1161)V; domIs355[mec-3p::QF, mec-4p::QS, QUAS::CoCHR, unc122p::RFP] ;zwIs108[myo-3p::Myc::unc-68 + myo-3p::GFP]*	This paper	N/A
C. elegans: *DAG747 unc-68(r1161)V; ljEx19[egl-46p::YC2.3; lin15(+)]*	This paper	N/A

C. elegans: *DAG792 egl-19(n582) IV; ljEx19[egl-46p::YC2.3; lin15(+)]*	This paper	N/A
C. elegans: *DAG795 cca-1(ad1650) X; ljEx19[egl-46p::YC2.3; lin15(+)]*	This paper	N/A
C. elegans: DAG885 *unc-77(gk9) IV; ljEx19[egl-46p::YC2.3; lin15(+)]*	This paper	N/A
C. elegans: DAG886 *nca-2(gk5) III ljEx19[egl-46p::YC2.3; lin15(+)]*	This paper	N/A
C. elegans: *DAG918 ocr-2(ak47) IV; ljEx19[egl-46p::YC2.3; lin15(+)]*	This paper	N/A
C. elegans: *DAG1000 domEx720[egl-46p::QF, QUAS::YC2.3(E31Q), unc122p::RFP].*	This paper	N/A
C. elegans: *DAG1001 unc-2(ra612) X; ljEx19[egl-46p::YC2.3; lin15(+)]*	This paper	N/A
C. elegans: *DAG1075 egl-3 (gk238) V; ljEx19[egl-46p::YC2.3; lin15(+)]*	This paper	N/A
C. elegans: *DAG1084 unc-13(e450) I; ljEx19[egl-46p::YC2.3; lin15(+)]*	This paper	N/A
Oligonucleotides		
Primer: egl-46pF: ggggacaactttgtatagaaaagttgatgttacaaattctcgaacaggt	This paper	N/A
Primer: egl-46pR: ggggactgctttttgtacaaacttgtggccttctgaaatcaaaac	This paper	N/A
Primer: YC2.3AttB1: ggggacaagtttgtacaaaaaagcaggcttcaccatggtgagcaagggcg	This paper	N/A
Primer: YC2.3AttB2: ggggaccactttgtacaagaaagctgggttacttgtacagctcgtccatgcc	This paper	N/A
Primer: E31QF: caacttggcaccgttatgaggtcg	This paper	N/A
Primer: E31QR: ctttgtggtgatggtgccgtc	This paper	N/A
Recombinant DNA		
Plasmid: pMH473 *[slot3 Entry unc-54 3'UTR*	Gift from Marc Hammarlund	N/A
Plasmid: coel::RFP *[unc-122p:.RFP]*	(Miyabayashi et al., 1999)	Addgene plasmid # 8938
Plasmid: dg229 *[slot1 Entry QUAS promoter]*	(Schild et al., 2014)	N/A
Plasmid: dg240 *[slot2 Entry QF]*	(Schild et al., 2014)	N/A
Plasmid: dg69 *[slot1 Entry egl-46 promoter]*	This paper	N/A
Plasmid: dg277 *[egl-46p::QF::unc-54-3'UTR]*	This paper	N/A
Plasmid: dg718 *[slot2 Entry YC2.3]*	This paper	N/A
Plasmid: dg719 *[slot2 Entry YC2.3(E31Q)]*	This paper	N/A
Plasmid: dg720 *[QUAS::YC2.3(E31Q)::unc-54-3'UTR]*	This paper	N/A

References

AOKI, I. & MORI, I. 2015. Molecular biology of thermosensory transduction in C. elegans. *Curr Opin Neurobiol,* 34**,** 117-24.

BACHNOFF, N., COHEN-KUTNER, M., TRUS, M. & ATLAS, D. 2013. Intra-membrane signaling between the voltage-gated Ca2+-channel and cysteine residues of syntaxin 1A coordinates synchronous release. *Sci Rep,* 3**,** 1620.

BUSCH, K. E., LAURENT, P., SOLTESZ, Z., MURPHY, R. J., FAIVRE, O., HEDWIG, B., THOMAS, M., SMITH, H. L. & DE BONO, M. 2012. Tonic signaling from O(2) sensors sets neural circuit activity and behavioral state. *Nat Neurosci,* 15**,** 581-91.

CHATZIGEORGIOU, M. & SCHAFER, W. R. 2011. Lateral facilitation between primary mechanosensory neurons controls nose touch perception in C. elegans. *Neuron,* 70**,** 299-309.

CHATZIGEORGIOU, M., YOO, S., WATSON, J. D., LEE, W. H., SPENCER, W. C., KINDT, K. S., HWANG, S. W., MILLER, D. M., 3RD, TREININ, M., DRISCOLL, M. & SCHAFER, W. R. 2010. Specific roles for DEG/ENaC and TRP channels in touch and thermosensation in C. elegans nociceptors. *Nat Neurosci,* 13**,** 861-8.

CHEN, C. L., BROOM, D. C., LIU, Y., DE NOOIJ, J. C., LI, Z., CEN, C., SAMAD, O. A., JESSELL, T. M., WOOLF, C. J. & MA, Q. 2006. Runx1 determines nociceptive sensory neuron phenotype and is required for thermal and neuropathic pain. *Neuron,* 49**,** 365-77.

CHIZH, B. A. & ILLES, P. 2001. P2X receptors and nociception. *Pharmacol Rev,* 53**,** 553-68.

CHUNG, S. H., CLARK, D. A., GABEL, C. V., MAZUR, E. & SAMUEL, A. D. 2006. The role of the AFD neuron in C. elegans thermotaxis analyzed using femtosecond laser ablation. *BMC Neurosci,* 7**,** 30.

CLARK, D. A., BIRON, D., SENGUPTA, P. & SAMUEL, A. D. 2006. The AFD sensory neurons encode multiple functions underlying thermotactic behavior in Caenorhabditis elegans. *J Neurosci,* 26**,** 7444-51.

COCHET-BISSUEL, M., LORY, P. & MONTEIL, A. 2014. The sodium leak channel, NALCN, in health and disease. *Front Cell Neurosci,* 8**,** 132.

CREGG, R., MOMIN, A., RUGIERO, F., WOOD, J. N. & ZHAO, J. 2010. Pain channelopathies. *J Physiol,* 588**,** 1897-904.

DE MORAES, E. R., KUSHMERICK, C. & NAVES, L. A. 2017. Morphological and functional diversity of first-order somatosensory neurons. *Biophys Rev,* 9**,** 847-856.

DIXON, R. E., YUAN, C., CHENG, E. P., NAVEDO, M. F. & SANTANA, L. F. 2012. Ca2+ signaling amplification by oligomerization of L-type Cav1.2 channels. *Proc Natl Acad Sci U S A,* 109**,** 1749-54.

DU, X. & GAMPER, N. 2013. Potassium channels in peripheral pain pathways: expression, function and therapeutic potential. *Curr Neuropharmacol,* 11**,** 621-40.

DUBIN, A. E. & PATAPOUTIAN, A. 2010. Nociceptors: the sensors of the pain pathway. *Journal of Clinical Investigation,* 120**,** 3760-3772.

EVANS, T. C. 2006. Transformation and microinjection. *WormBook,* 10.

FORD, N. C., REN, D. & BACCEI, M. L. 2018. NALCN channels enhance the intrinsic excitability of spinal projection neurons. *Pain,* 159**,** 1719-1730.

GASCON, E. & MOQRICH, A. 2010. Heterogeneity in primary nociceptive neurons: from molecules to pathology. *Arch Pharm Res,* 33**,** 1489-507.

GEFFENEY, S. L., CUEVA, J. G., GLAUSER, D. A., DOLL, J. C., LEE, T. H., MONTOYA, M., KARANIA, S., GARAKANI, A. M., PRUITT, B. L. & GOODMAN, M. B. 2011. DEG/ENaC but not TRP channels are the major mechanoelectrical transduction channels in a C. elegans nociceptor. *Neuron,* 71**,** 845-57.

GIRARD, L. R., FIEDLER, T. J., HARRIS, T. W., CARVALHO, F., ANTOSHECHKIN, I., HAN, M., STERNBERG, P. W., STEIN, L. D. & CHALFIE, M. 2007. WormBook: the online review of Caenorhabditis elegans biology. *Nucleic Acids Res,* 35**,** D472-5.

GLAUSER, D. A. 2013. How and why Caenorhabditis elegans uses distinct escape and avoidance regimes to minimize exposure to noxious heat. *Worm,* 2**,** e27285.

GLAUSER, D. A., CHEN, W. C., AGIN, R., MACINNIS, B. L., HELLMAN, A. B., GARRITY, P. A., TAN, M. W. & GOODMAN, M. B. 2011. Heat avoidance is regulated by transient receptor potential (TRP) channels and a neuropeptide signaling pathway in Caenorhabditis elegans. *Genetics,* 188**,** 91-103.

GOLD, M. S. & GEBHART, G. F. 2010. Nociceptor sensitization in pain pathogenesis. *Nat Med,* 16**,** 1248-57.

GOODMAN, M. B. & SENGUPTA, P. 2018. The extraordinary AFD thermosensor of C. elegans. *Pflugers Arch,* 470**,** 839-849.

HAWK, J. D., CALVO, A. C., LIU, P., ALMORIL-PORRAS, A., ALJOBEH, A., TORRUELLA-SUAREZ, M. L., REN, I., COOK, N., GREENWOOD, J., LUO, L., WANG, Z. W., SAMUEL, A. D. T. & COLON-RAMOS, D. A. 2018. Integration of Plasticity Mechanisms within a Single Sensory Neuron of C. elegans Actuates a Memory. *Neuron,* 97**,** 356-367 e4.

HEDGECOCK, E. M. & RUSSELL, R. L. 1975. Normal and mutant thermotaxis in the nematode Caenorhabditis elegans. *Proc Natl Acad Sci U S A,* 72**,** 4061-5.

HILLIARD, M. A., APICELLA, A. J., KERR, R., SUZUKI, H., BAZZICALUPO, P. & SCHAFER, W. R. 2005. In vivo imaging of C. elegans ASH neurons: cellular response and adaptation to chemical repellents. *EMBO J,* 24**,** 63-72.

HOBERT, O. 2013. The neuronal genome of Caenorhabditis elegans. *WormBook***,** 1-106.

JOSPIN, M., WATANABE, S., JOSHI, D., YOUNG, S., HAMMING, K., THACKER, C., SNUTCH, T. P., JORGENSEN, E. M. & SCHUSKE, K. 2007. UNC-80 and the NCA ion channels contribute to endocytosis defects in synaptojanin mutants. *Curr Biol,* 17**,** 1595-600.

KOTERA, I., TRAN, N. A., FU, D., KIM, J. H., BYRNE RODGERS, J. & RYU, W. S. 2016. Pan-neuronal screening in Caenorhabditis elegans reveals asymmetric dynamics of AWC neurons is critical for thermal avoidance behavior. *eLife,* 5**,** e19021.

LI, W., KANG, L., PIGGOTT, B. J., FENG, Z. & XU, X. Z. 2011. The neural circuits and sensory channels mediating harsh touch sensation in Caenorhabditis elegans. *Nat Commun,* 2**,** 315.

LIU, S., SCHULZE, E. & BAUMEISTER, R. 2012. Temperature- and touch-sensitive neurons couple CNG and TRPV channel activities to control heat avoidance in Caenorhabditis elegans. *PLoS One,* 7**,** e32360.

LU, B., SU, Y., DAS, S., LIU, J., XIA, J. & REN, D. 2007. The neuronal channel NALCN contributes resting sodium permeability and is required for normal respiratory rhythm. *Cell,* 129**,** 371-83.

MIYABAYASHI, T., PALFREYMAN, M. T., SLUDER, A. E., SLACK, F. & SENGUPTA, P. 1999. Expression and function of members of a divergent nuclear receptor family in Caenorhabditis elegans. *Dev Biol,* 215**,** 314-31.

MOHAMMADI, A., BYRNE RODGERS, J., KOTERA, I. & RYU, W. S. 2013. Behavioral response of Caenorhabditis elegans to localized thermal stimuli. *BMC Neurosci,* 14**,** 66.

NAGEL, G., BRAUNER, M., LIEWALD, J. F., ADEISHVILI, N., BAMBERG, E. & GOTTSCHALK, A. 2005. Light activation of channelrhodopsin-2 in excitable cells of Caenorhabditis elegans triggers rapid behavioral responses. *Curr Biol,* 15**,** 2279-84.

PARK, J. & LUO, Z. D. 2010. Calcium channel functions in pain processing. *Channels (Austin),* 4**,** 510-7.

PATERNOSTER, R., BRAME, R., MAZEROLLE, P. & PIQUERO, A. 1998. Using the correct statistical test for the equality of regression coefficients. *Criminology,* 36**,** 859-866.

RAMSEY, I. S., DELLING, M. & CLAPHAM, D. E. 2006. An introduction to TRP channels. *Annu Rev Physiol,* 68**,** 619-47.

RAOUF, R., QUICK, K. & WOOD, J. N. 2010. Pain as a channelopathy. *J Clin Invest,* 120**,** 3745-52.

RODERICK, H. L., BERRIDGE, M. J. & BOOTMAN, M. D. 2003. Calcium-induced calcium release. *Curr Biol,* 13**,** R425.

SALKOFF, L., WEI, A., BABAN, B., BUTLER, A., FAWCETT, G., G, F. & SANTI, C. 2005. Potassium channels in C. elegans. *WormBook*.

SCHILD, L. C. & GLAUSER, D. A. 2013. Dynamic switching between escape and avoidance regimes reduces Caenorhabditis elegans exposure to noxious heat. *Nat Commun,* 4**,** 2198.

SCHILD, L. C. & GLAUSER, D. A. 2015. Dual Color Neural Activation and Behavior Control with Chrimson and CoChR in Caenorhabditis elegans. *Genetics,* 200**,** 1029-34.

SCHILD, L. C., ZBINDEN, L., BELL, H. W., YU, Y. V., SENGUPTA, P., GOODMAN, M. B. & GLAUSER, D. A. 2014. The balance between cytoplasmic and nuclear CaM kinase-1 signaling controls the operating range of noxious heat avoidance. *Neuron,* 84**,** 983-96.

SWIERCZEK, N. A., GILES, A. C., RANKIN, C. H. & KERR, R. A. 2011. High-throughput behavioral analysis in C. elegans. *Nat Methods,* 8**,** 592-8.

VRIENS, J., NILIUS, B. & VOETS, T. 2014. Peripheral thermosensation in mammals. *Nat Rev Neurosci,* 15**,** 573-89.

WEMMIE, J. A., TAUGHER, R. J. & KREPLE, C. J. 2013. Acid-sensing ion channels in pain and disease. *Nat Rev Neurosci,* 14**,** 461-71.

WHITE, J. G., SOUTHGATE, E., THOMSON, J. N. & BRENNER, S. 1986. The structure of the nervous system of the nematode Caenorhabditis elegans. *Philos Trans R Soc Lond B Biol Sci,* 314**,** 1-340.

WITTENBURG, N. & BAUMEISTER, R. 1999. Thermal avoidance in Caenorhabditis elegans: an approach to the study of nociception. *Proc Natl Acad Sci U S A,* 96**,** 10477-82.

WOOD, J. N., BOORMAN, J. P., OKUSE, K. & BAKER, M. D. 2004. Voltage-gated sodium channels and pain pathways. *J Neurobiol,* 61**,** 55-71.

WOOLF, C. J. & MA, Q. 2007. Nociceptors--noxious stimulus detectors. *Neuron,* 55**,** 353-64.

YEH, E., NG, S., ZHANG, M., BOUHOURS, M., WANG, Y., WANG, M., HUNG, W., AOYAGI, K., MELNIK-MARTINEZ, K., LI, M., LIU, F., SCHAFER, W. R. & ZHEN, M. 2008. A putative cation channel, NCA-1, and a novel protein, UNC-80, transmit neuronal activity in C. elegans. *PLoS Biol,* 6**,** e55.

YU, Y. Q., CHEN, X. F., YANG, Y., YANG, F. & CHEN, J. 2014. Electrophysiological identification of tonic and phasic neurons in sensory dorsal root ganglion and their distinct implications in inflammatory pain. *Physiol Res,* 63**,** 793-9.

ZHENG, J. 2013. Molecular Mechanism of TRP Channels. *Comprehensive Physiology,* 3**,** 221-242.

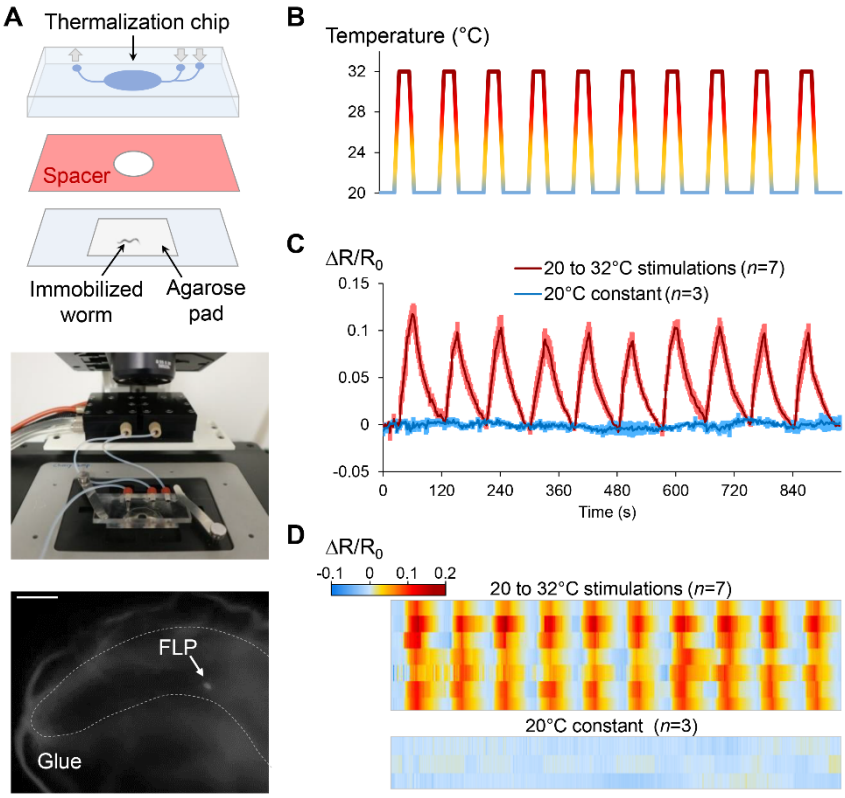
A
Thermalization chip
Spacer
Immobilized worm
Agarose pad
FLP
Glue
B
Temperature (°C)
32
28
24
20
C
ΔR/R0
20 to 32°C stimulations (n=7)
20°C constant (n=3)
0.15
0.1
0.05
0
-0.05
0
120
240
360
480
600
720
840
Time (s)
D
ΔR/R0
-0.1
0
0.1
0.2
20 to 32°C stimulations (n=7)
20°C constant (n=3)

Fig 1

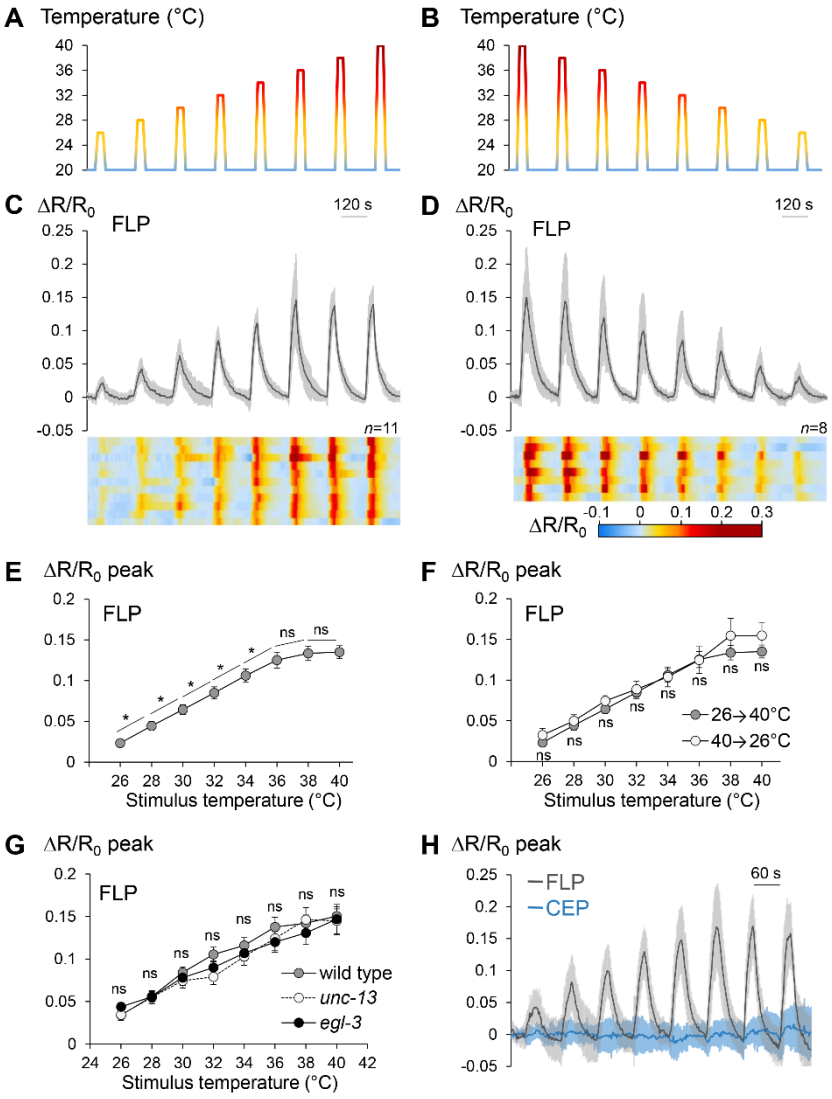
A Temperature (°C)
B Temperature (°C)
C ΔR/R0
FLP
120 s
n=11
D ΔR/R0
FLP
120 s
n=8
ΔR/R0
E ΔR/R0 peak
FLP
Stimulus temperature (°C)
F ΔR/R0 peak
FLP
26→40°C
40→26°C
Stimulus temperature (°C)
G ΔR/R0 peak
FLP
wild type
unc-13
egl-3
Stimulus temperature (°C)
H ΔR/R0 peak
FLP
CEP
60 s

Fig 2

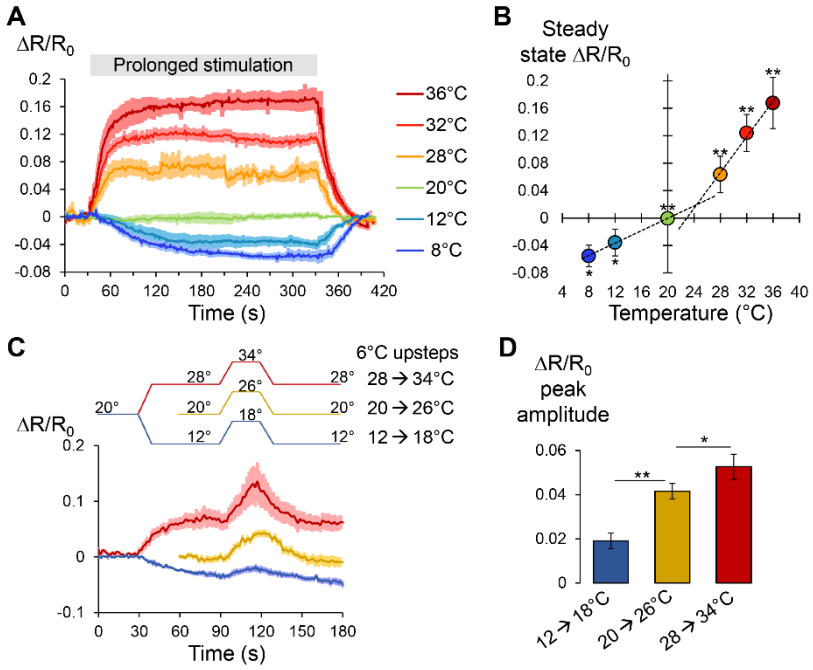
A
ΔR/R0
Prolonged stimulation
36°C
32°C
28°C
20°C
12°C
8°C
Time (s)
B
Steady state ΔR/R0
Temperature (°C)
C
6°C upsteps
28 → 34°C
20 → 26°C
12 → 18°C
ΔR/R0
Time (s)
D
ΔR/R0 peak amplitude
12 → 18°C
20 → 26°C
28 → 34°C

Fig 3

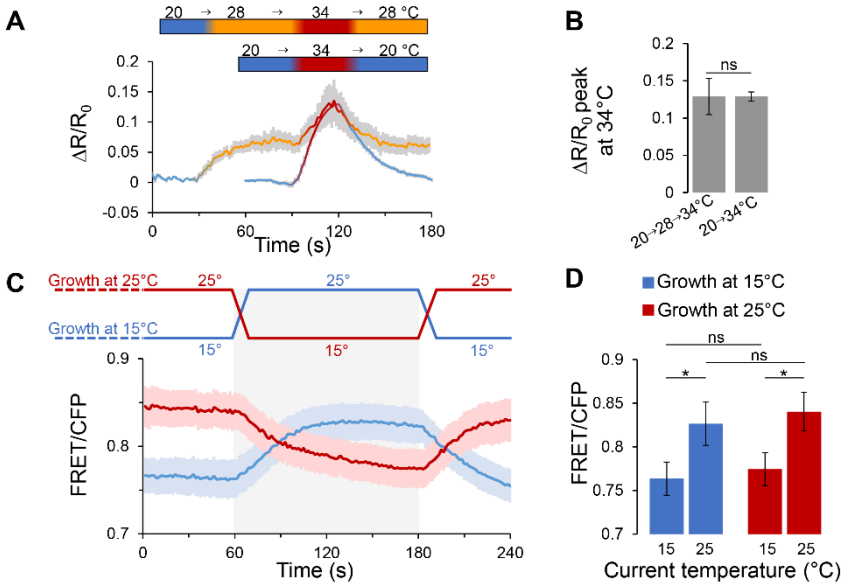
A
20 → 28 → 34 → 28 °C
20 → 34 → 20 °C
ΔR/R0
Time (s)
B
ΔR/R0 peak at 34°C
ns
20→28→34°C
20→34°C
C
Growth at 25°C
Growth at 15°C
25°
15°
FRET/CFP
Time (s)
D
Growth at 15°C
Growth at 25°C
ns
*
FRET/CFP
Current temperature (°C)

FIg 4

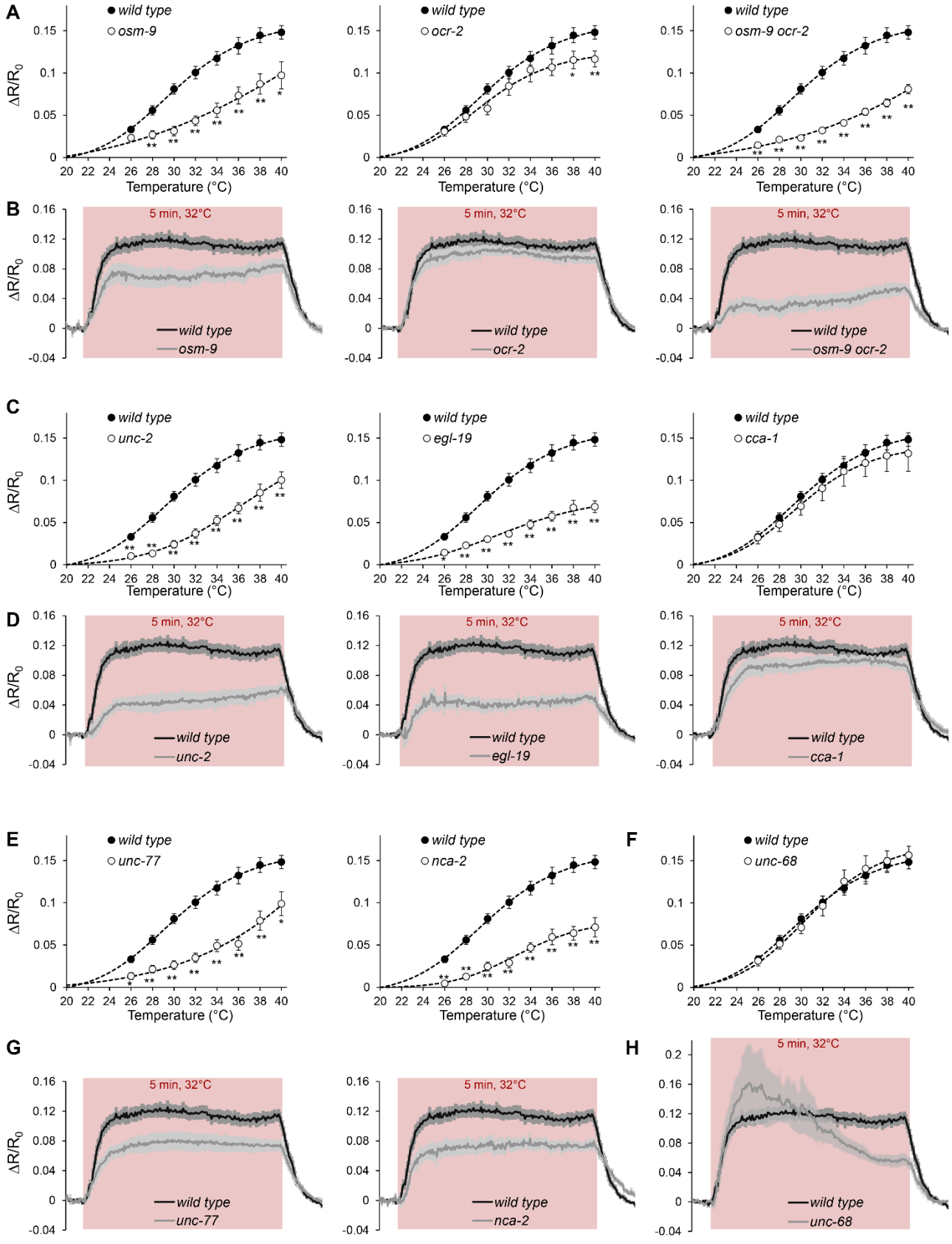
A
wild type
osm-9
ocr-2
osm-9 ocr-2
ΔR/R0
Temperature (°C)
B
5 min, 32°C
wild type
osm-9
ocr-2
osm-9 ocr-2
C
unc-2
egl-19
cca-1
D
unc-2
egl-19
cca-1
E
unc-77
nca-2
F
unc-68
G
unc-77
nca-2
H
unc-68

FIg 5

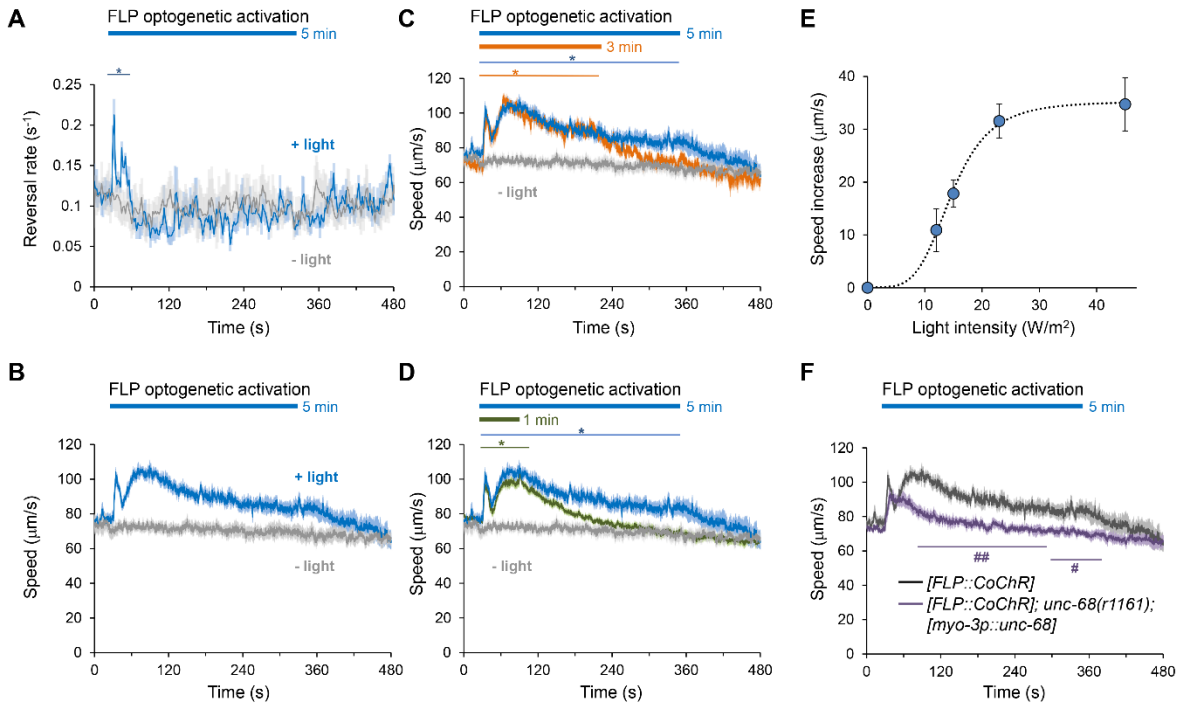
A
FLP optogenetic activation
5 min
Reversal rate (s-1)
+ light
- light
Time (s)
B
FLP optogenetic activation
5 min
Speed (µm/s)
+ light
- light
Time (s)
C
FLP optogenetic activation
5 min
3 min
Speed (µm/s)
- light
Time (s)
D
FLP optogenetic activation
5 min
1 min
Speed (µm/s)
- light
Time (s)
E
Speed increase (µm/s)
Light intensity (W/m2)
F
FLP optogenetic activation
5 min
Speed (µm/s)
##
#
[FLP::CoChR]
[FLP::CoChR]; unc-68(r1161);
[myo-3p::unc-68]
Time (s)

Fig 6

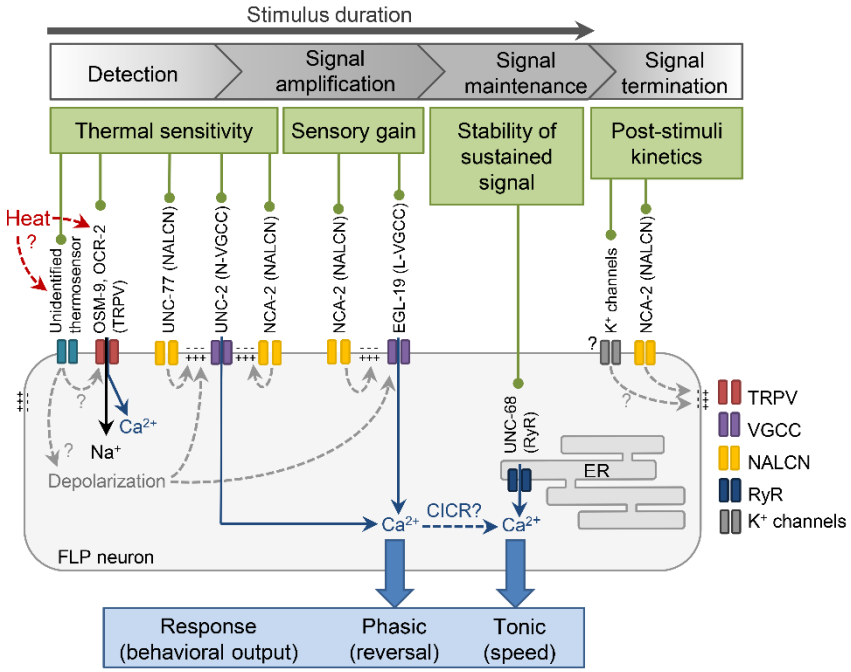
Stimulus duration
Detection
Signal amplification
Signal maintenance
Signal termination
Thermal sensitivity
Sensory gain
Stability of sustained signal
Post-stimuli kinetics
Heat
?
Unidentified thermosensor
OSM-9, OCR-2 (TRPV)
UNC-77 (NALCN)
UNC-2 (N-VGCC)
NCA-2 (NALCN)
NCA-2 (NALCN)
EGL-19 (L-VGCC)
K+ channels
NCA-2 (NALCN)
Ca2+
Na+
Depolarization
UNC-68 (RyR)
ER
CICR?
Ca2+
Ca2+
FLP neuron
TRPV
VGCC
NALCN
RyR
K+ channels
Response (behavioral output)
Phasic (reversal)
Tonic (speed)

Fig 7

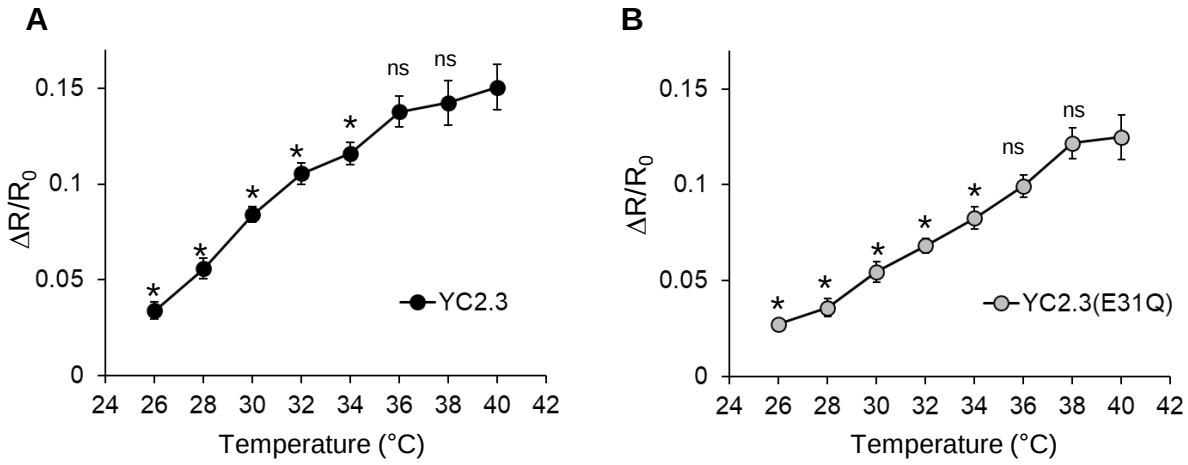

Figure S1 Similar FLP calcium response plateau with both YC2.3 and low calcium affinity mutant sensor YC2.3(E31Q), Related to Figure 2. Average peak calcium responses in FLP cell bodies expressing the YC2.3 (**A**) or YC2.3(E31Q) (**B**) sensors, respectively, and stimulated as in Figure 2H. Error bars are SEM; $n \geq 11$ animals. ns, not significant; *, $p < .05$ vs maximal peak at 40°C by Student's *t*-tests.

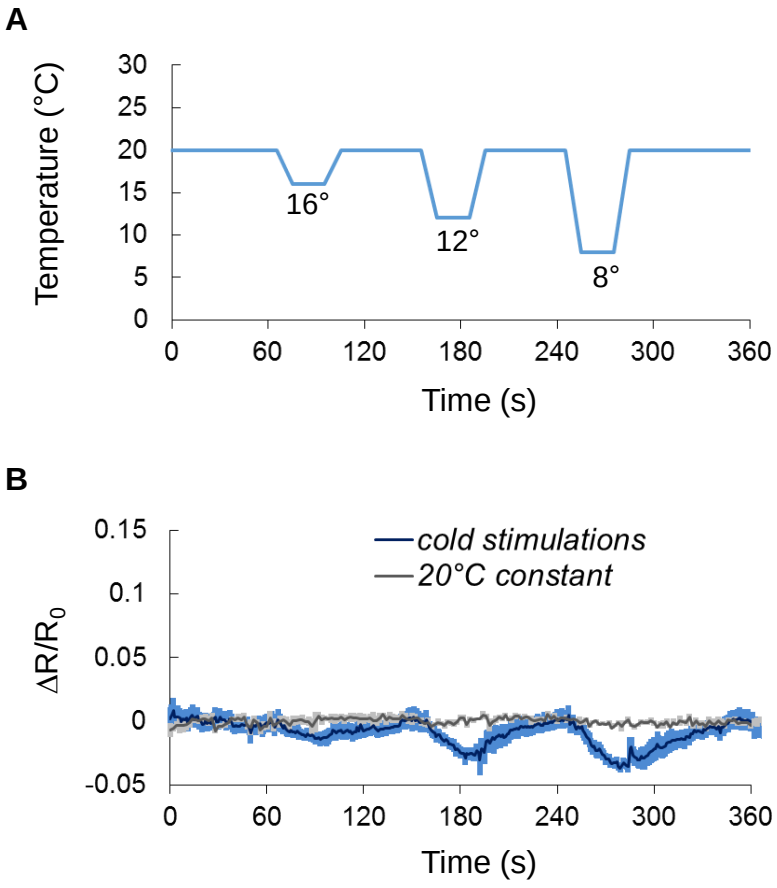

Figure S2. Effect of short cold stimuli on FLP calcium activity, Related to Figure 3
(**A**) Stimulation protocol with short (30 s) cold pulses at 16°C, 12°C and 8°C, with 60 s ISI. Baseline was 20°C. (**B**) FLP calcium response to cold stimuli (blue) compared to calcium levels in constant 20°C temperature (grey). Lines indicate the averages, shades the SEM. *n=5*. To ease comparison, the scale of the vertical axis was kept similar to that in Fig. 3.

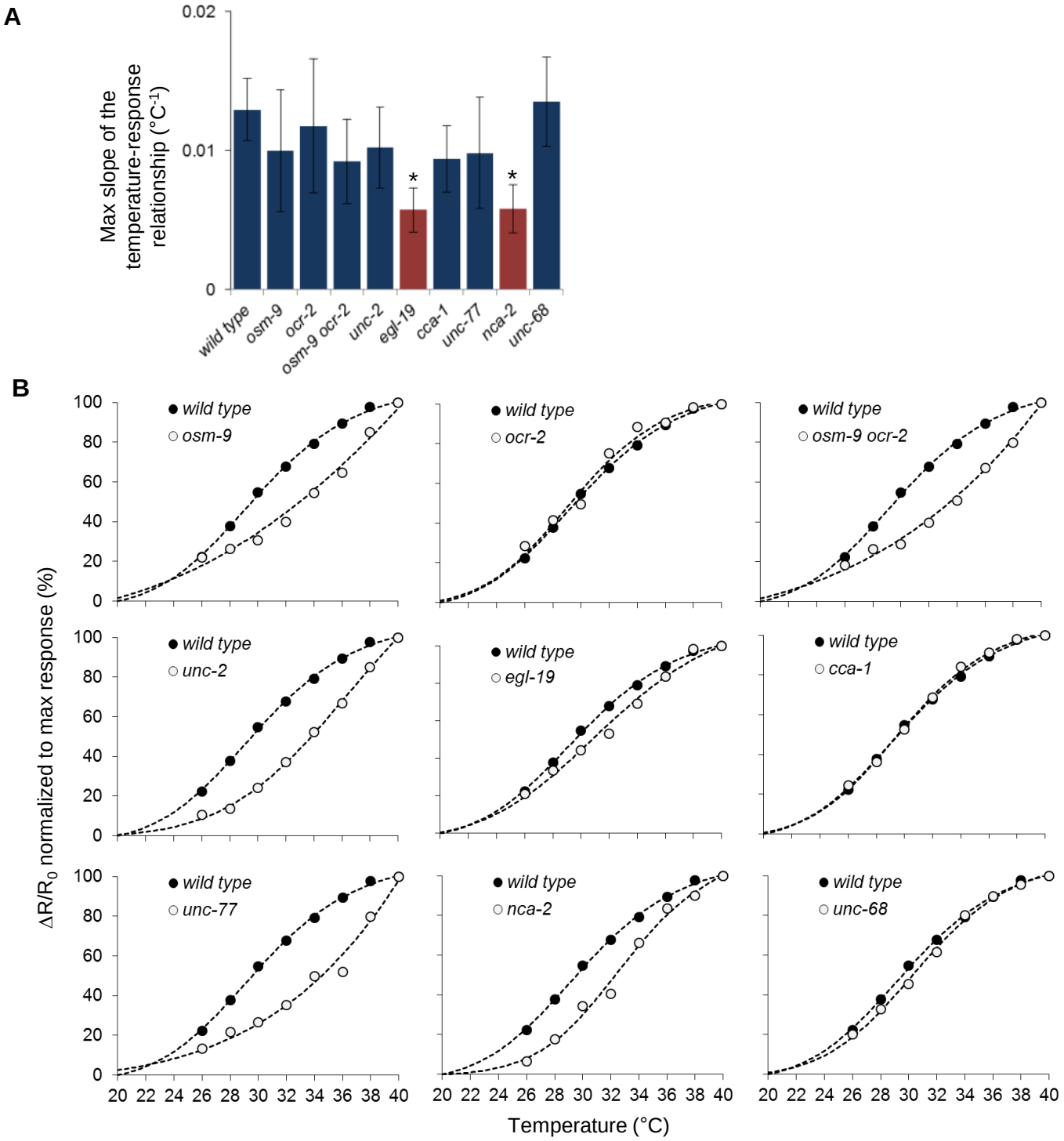

Figure S3 Noxious heat-evoked FLP calcium responses in ion channel mutants: temperature-response curve analyses, Related to Figure 5. Heat dose responses in wild type and indicated mutants: *osm-9(ky10)*, *ocr-2(ak47)*, *osm-9(ky10)ocr-2(ak47)*, *unc-2(ra612)*, *egl-19(n582)*, *cca-1(ad1650)*, *unc-77(gk9)*, *nca-2(gk5)* and *unc-68(r1161).* (**A**) Maximal slope of the temperature-response ($\Delta R/R_0$) curves from the data in Figure 5. One way ANOVA indicated a significant genotype effect. *, $p<.01$ as compared to wild type by Bonferroni post-hoc tests. (**B**) Normalized $\Delta R/R_0$ to the maximal response for each genotype (% of max response) from data in Figure 5. Dotted lines indicate sigmoid curve fittings.

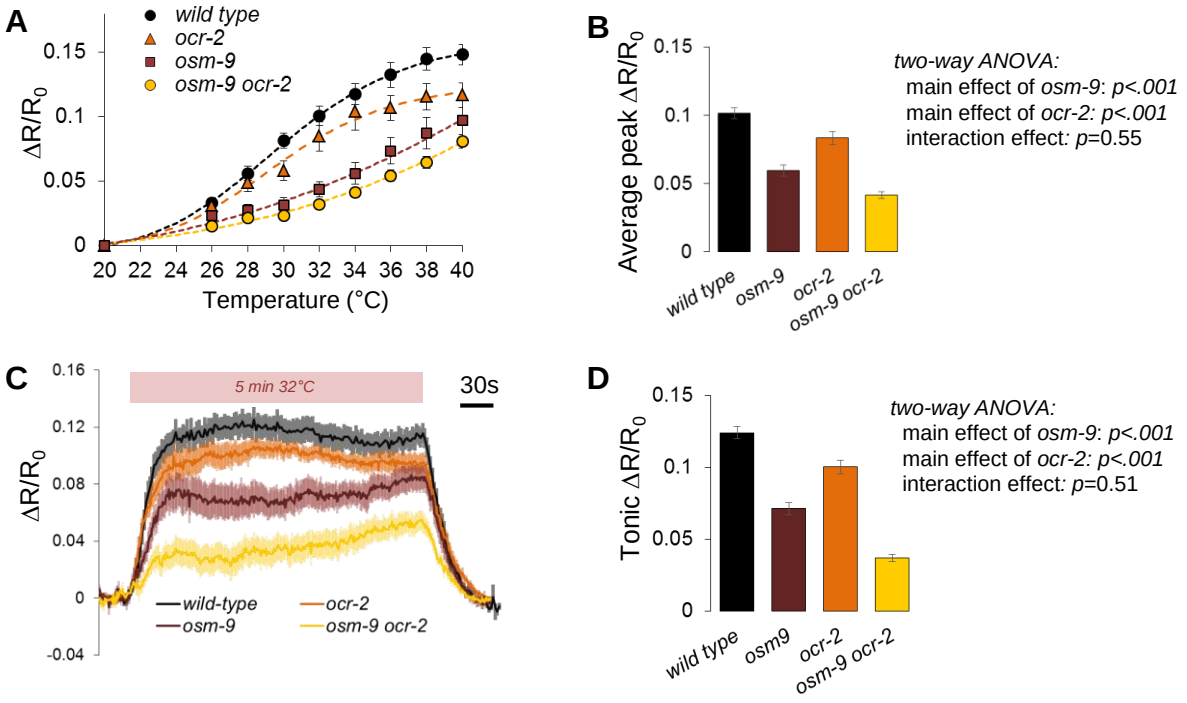

Figure S4: Cumulative impact of *osm-9* and *ocr-2* on noxious heat-evoked FLP calcium responses, Related to Figure 5.

(**A**) Heat-evoked calcium peaks in FLP cell bodies as a function of stimulus intensity in wild type and mutants: *osm-9(ky10)*, *ocr-2(ak47)*, *osm-9(ky10);ocr-2(ak47).* Same data as in Fig. 5a pooled on a single plot. Each dot represents the average $\Delta R/R_0$ peak amplitude reached upon 30 s stimuli from a baseline at 20°C (as in Fig. 2H). SEM as error bars. Dotted lines indicate 4-parameter sigmoid curve fittings. *n*≥10 independent recordings, each in a different animal.

(**B**) Calcium peaks averaged on all thermal stimuli for each genotype from panel **A** (error bars indicate SEM) and results of a two-way ANOVA with *osm-9* allele and *ocr-2* allele as factors.

(**C**) Heat-evoked tonic calcium responses in FLP cell bodies in wild type and indicated mutants. Same data as in Fig. 5B pooled on a single plot. Solid lines indicate the averages, shades indicate the SEM, *n*≥10 independent recordings, each in a different animal.

(**D**) Calcium change during the tonic stimulation averaged over the 120s to 300s period from data in panel **C** (error bars indicate SEM) and results of a two-way ANOVA with *osm-9* allele and *ocr-2* allele as factors.

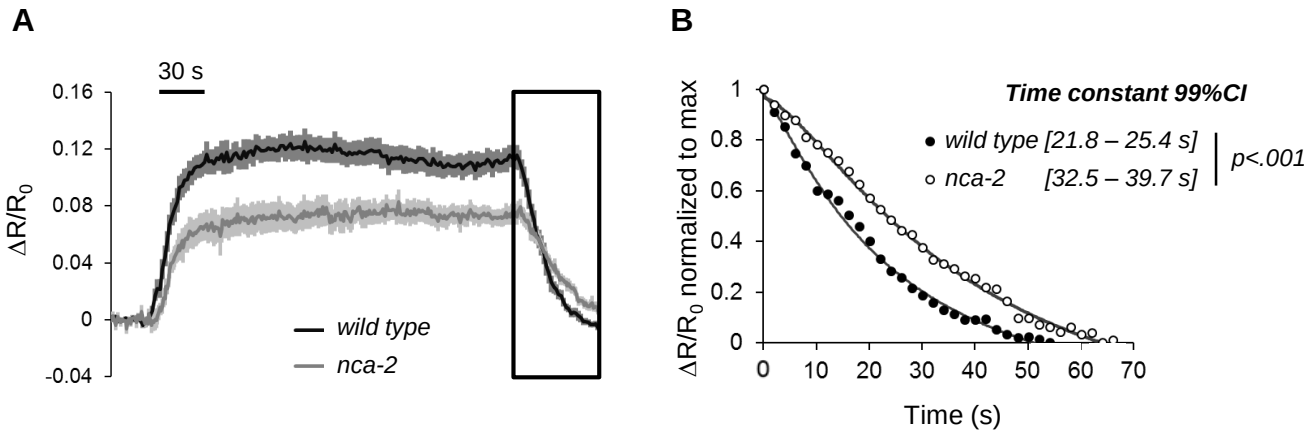

Figure S5. Kinetic analysis in *nca-2(gk5)* mutant animals, Related to Figure 5. (**A**) Tonic response profiles upon 5 min sustained stimulation. Data are the same as in Fig. 5G. Post-stimulus recovery period is highlighted. Lines indicate averages, shades are SEM. *n*≥10. (**B**) Detailed kinetic analysis and direct comparison with wild type decay response, with response maximal signal at time 0 normalized to 1. Dots indicate averages, lines are sigmoid fitting curves, *n*≥10. Time constant were estimated from the sigmoid fitting and 99% confidence intervals (99%CI) are indicated for each genotype.

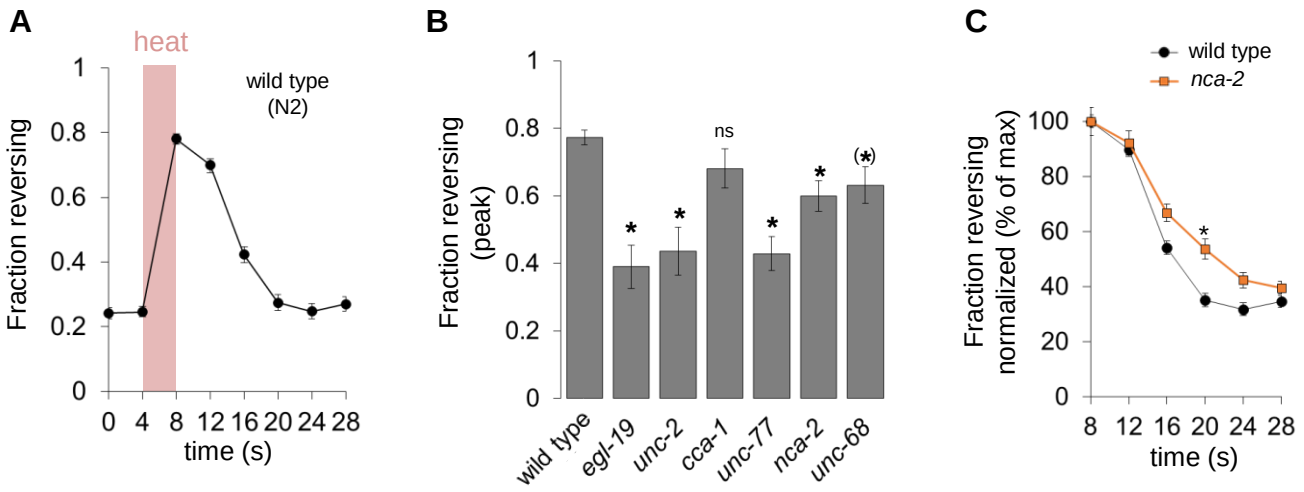

Figure S6. Specific mutations affect the reversal response induced by short heat stimuli, related to Figure 5. (**A**) Temporal unfolding of acute reversal induction with a 4 s heat stimulus producing a ~1.5 °C/s thermal increase (as indicated with the red shade) in wild type. Average +/- SEM, *n*= 26 plate recordings, each containing at least 50 worms. (**B**) Wild type and mutant peak reversal responses recorded as in **A**. L-type VGCC: *egl-19(n582)*; N-type VGCC: *unc-2(ra612)*; T-type VGCC: *cca-1(ad1650)*; NALCNs: *unc-77(gk9)*, *nca-2(gk5)*; RYR: *unc-68(r1161).* Bars represent averages of *n*≥7 plate recordings, each containing at least 50 worms. Error bars are SEM. Significant genotype effect with one-way ANOVA; *, *p*<.01, (*) *p*<.05 vs wild type by Bonferroni post-hoc tests. (**C**) Detailed comparison of the reversal rate decay kinetics in the post-stimulus period in wild type and *nca-2* mutants. Reversal rate is normalized to the maximal response rate in each genotype. Two-way ANOVA showed a significant genotype x time interaction. *, *p*<.01 vs wild type by Bonferroni post-hoc tests.

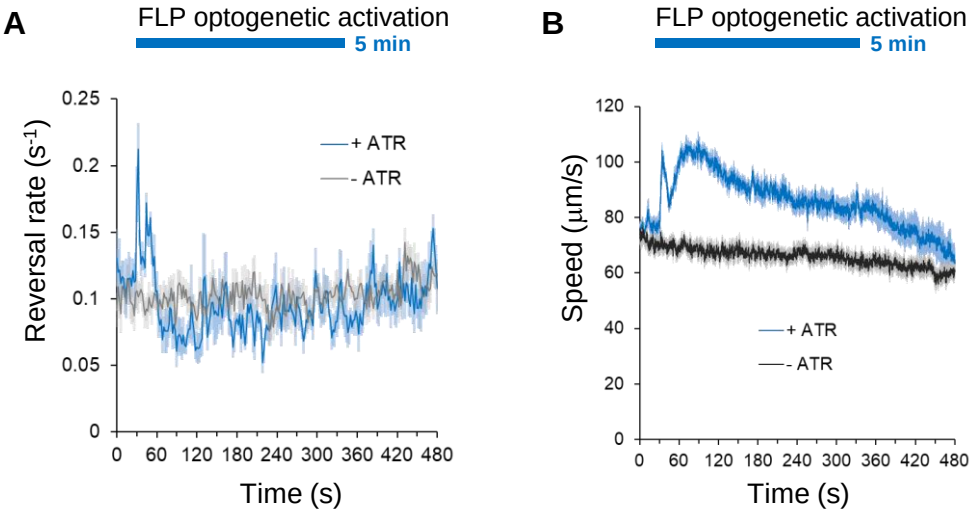

Figure S7. Behavioral responses to sustained FLP optogenetic stimulations require ATR, related to Figure 6.

(**A, B**) Reversal and speed responses in *domIs355[FLP::CoChR]* animals grown in the presence (+ATR) or the absence (-ATR) of all-*trans*-retinal (ATR), and exposed for 5 minutes to 15 W/m^2 of blue light. *n>5* independent plate recordings, each tracking at least 50 animals.